Leckie, R.M., Sigurdsson, H., Acton, G.D., and Draper, G. (Eds.), 2000
Proceedings of the Ocean Drilling Program, Scientific Results, Vol. 165

20. HISTORY OF CIRCUM-CARIBBEAN EXPLOSIVE VOLCANISM: $^{40}Ar/^{39}Ar$ DATING OF TEPHRA LAYERS[1]

H. Sigurdsson,[2] S. Kelley,[3] R.M. Leckie,[4] S. Carey,[2] T. Bralower,[5] and J. King[2]

ABSTRACT

Drilling in the Caribbean Sea during Ocean Drilling Program Leg 165 has recovered a large number of silicic tephra layers and led to the discovery of three major episodes of explosive volcanism that occurred during the last 55 m.y. on the margins of this evolving ocean basin. The earliest episode is marked by Paleocene to early Eocene explosive volcanism on the Cayman Rise, associated with activity of the Cayman arc, an island arc that was the westward extension of the Sierra Maestra volcanic arc in southern Cuba. Caribbean sediments also document a major mid- to late Eocene explosive volcanic episode that is attributed to ignimbrite-forming eruptions on the Chortis Block in Central America to the west. This event is contemporaneous with the first phase of activity of the Sierra Madre volcanic episode in Mexico, the largest ignimbrite province on Earth. In the Caribbean sediments, a Miocene episode of explosive volcanism is comparable to the Eocene event, and also attributed to sources in the Central American arc to the west. Radiometric $^{40}Ar/^{39}Ar$ dates have been obtained for biotites and sanidines from 27 tephra layers, providing absolute ages for the volcanic episodes and further constraining the geochronology of Caribbean sediments. Volcanic activity of the Cayman arc is attributed to the northward subduction of the leading edge of the oceanic plate that carried the Caribbean oceanic plateau. Although the factors generating the large episodes of Central American explosive volcanism are unclear, we propose that they are related to contemporary major readjustments of plate tectonic configuration in the Pacific.

INTRODUCTION

Explosive volcanism plays a fundamental role in the exchange of mass and energy between the solid Earth and the oceans and atmosphere. Large-scale silicic eruptions that generate voluminous pyroclastic flows (ignimbrite deposits) represent the largest type of volcanic event known on Earth. Individual eruptions may discharge up to several thousand cubic kilometers of magma during a single event (Chesner et al., 1991). Such events are of great interest, more over, because of their potential for global environmental change (Crowley et al., 1993). Large ignimbrite eruptions occur relatively infrequently (one event every 20,000 yr erupts a volume >1000 km^3), but significant uncertainties exist regarding variations in the rate of this type of volcanism on Earth or in a given volcanic province. Just as variations in mid-ocean ridge and plume activity have become the focus of intense study, there is a compelling need to examine long-term variations in volcanism associated with subduction zones, especially considering the potential that such events have for profound societal impact. Recognizing that the Earth's current state is not necessarily typical of all tectonic regimes in the past, it is important to study the long-term geochemical and tectonic evolution of the Earth system.

Unraveling the land-based record of volcanism in a major ignimbrite province is hampered by the paucity and poor precision of many radiometric age dates, lack of mappable stratigraphic levels, and poor preservation. Major explosive volcanic eruptions are, however, well preserved in the marine environment adjacent to subduction zones as volcanic ash, or tephra layers, interbedded with deep-sea sediments. The marine tephra record is condensed in thickness compared with the terrestrial one, but it is more likely to be complete, and easily dated by biostratigraphic methods and radiometric dating of phenocrysts found in the tephra layers.

Recent drilling during Leg 165 of the Ocean Drilling Program (ODP) in the Caribbean Sea (Fig. 1) yielded more than 2000 tephra layers, with individual layers up to 90 cm thick. This led to the discovery of three major episodes of Cenozoic explosive volcanism (Sigurdsson, Leckie, Acton, et al., 1997). These episodes, one during the early to mid-Miocene, another from the mid- to late Eocene and the earliest one in late Paleocene to early Eocene time, represent periods during which the rate of large-scale ignimbrite-forming eruptions was much greater than at present (Fig. 2). The excellent recovery of this record, in seven holes, allows for the study of the most complete sequence of long-term temporal changes in subduction zone volcanism through the Cenozoic Era. This unique tephra record can be used in order to quantify the nature and rates of volcanism during these three important episodes. In this paper we discuss the Leg 165 tephra record and relate it to the complex history of volcano-tectonic activity at the margins of the Caribbean plate. We also present new $^{40}Ar/^{39}Ar$ dates of biotite and feldspar crystals from a large number of Caribbean marine tephra layers, to provide further constraints of the timing of volcanism in the region.

ANALYTICAL METHODS

Tephra layers were selected for analysis on the basis of shipboard petrographic studies of smear slides, with emphasis placed on unaltered, biotite- and/or feldspar-bearing layers. Most of the layers are only partly consolidated and were easily disaggregated in an ultrasonic bath. The carbonate fraction was removed with mild acetic acid. The remaining glass, smectite, and phenocryst residue was wet-sieved. Under the stereo microscope, biotite phenocrysts were often conspicuous in the residue and were generally hand picked from the >63- or >125-µm size fractions (Fig. 3). Some biotites show signs of minor alteration, with development of chlorite at the edges of grains. Such grains were discarded whenever possible. Feldspar phenocrysts

[1]Leckie, R.M., Sigurdsson, H., Acton, G.D., and Draper, G. (Eds.), 2000. *Proc. ODP, Sci. Results,* 165: College Station, TX (Ocean Drilling Program).

[2]Graduate School of Oceanography, University of Rhode Island, Narragansett, RI 02882, U.S.A. haraldur@gsosun1.gso.uri.edu

[3]Department of Earth Sciences, The Open University, Milton Keynes, MK7 6AA, United Kingdom.

[4]Department of Geosciences, University of Massachusetts, Amherst, MA 01003, U.S.A.

[5]Department of Geological Sciences, University of North Carolina, Chapel Hill, NC 27599, U.S.A.

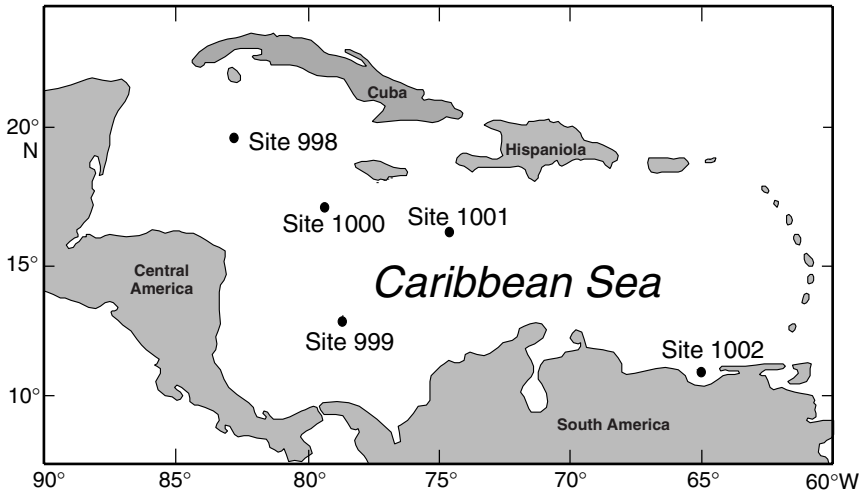

Figure 1. Location of sites drilled during Leg 165, discussed in the text.

are smaller and often difficult to distinguish from glass shards. In this case, feldspars were separated from glass shards using a lithium polytungstate heavy liquid.

The freshest, unfractured single grains were handpicked, packed in aluminum foil and sent for irradiation at either the Risö National Laboratory in Denmark or the research reactor at McMaster University, Canada. The age determinations were carried out at the Ar-Ar laboratory at the Earth Sciences Department, Open University, England. The laboratory is equipped with a Mass Analyzer Products 215–50 noble gas mass spectrometer with an automated extraction line. The system is equipped with a Johnston multiplier detector, dedicated to laser Ar-Ar dating, using a continuous infra-red (Nd-YAG) laser focused through a customized Leica Metallux 3 microscope. It is designed to measure small samples, either as single grains heated for 10–300 s or in situ in thick rock sections using millisecond pulses (Kelley, 1995). The laser is capable of delivering up to 70 W using the wider multimode beam, sufficient to melt and degas even sanidine. Upon return from irradiation, individual grains are loaded into small 2-mm diameter, 2-mm deep holes in an aluminum plate that is loaded into a ultra-high vacuum laser port with a fused silica window. Grains are heated individually or in small groups in 60-s heating steps using a defocused multimode laser.

Gas samples are accumulated for a minimum of 5 min and equilibrated into the MAP 215–50 noble gas mass spectrometer. All argon peaks are scanned 10 times, and peak heights are extrapolated back to the inlet time to take account of argon buildup and memory effects. The mean blank plus mass spectrometer backgrounds are currently 2.4, 0.02, and 0.3×10^{-12} cm^3 STP for ^{40}Ar, ^{39}Ar, and ^{36}Ar respectively. Raw data are corrected for mass spectrometer discrimination and irradiation interference reactions, which are monitored by irradiating calcium and potassium salts with the samples. A J-value is assigned to the samples, using the international biotite mineral standard GA1550 and its assigned age of 97.9 Ma (McDougall and Roksandic, 1974), and an internal biotite standard. Accuracy is difficult to determine, since there is controversy among Ar-Ar specialists about the precise age of the international standards. However, the largest uncertainty in the absolute accuracy is 1.25% at the 1 sigma level. Generally, the precision on the ages is better than 1% at the 2 sigma (95% confidence level). In the case of biotites dating from the Neogene, say 20 Ma, the error is probably 0.2 Ma or better, depending upon the amount of secondary chlorite in the biotite grains.

RESULTS

Biotites were hand picked from 27 tephra layers in Leg 165 cores for ^{40}Ar/^{39}Ar analysis. Up to 24 single crystal dates were obtained from each sample. The results of biotite analyses are presented in Table 1, where the weighted mean (weighted on the basis of the analytical error for each analysis) of the single crystal dates is adopted as the radiometric age of each tephra layer. Weighted means and errors were calculated on the basis of the method presented in Ludwig (1998).

The results of ^{40}Ar/^{39}Ar dating of Caribbean tephra layers are compared in Table 2 with the ages assigned to the sediments containing the tephra, on the basis of nannofossil and planktonic foraminiferal biochronology documented by the Leg 165 scientific party and subsequent shore-based studies (Sigurdsson, Leckie, Acton, et al., 1997; Chaisson and D'Hondt, Chap. 2, this volume; Kameo and Bralower, Chap. 1, this volume). In general, each of the 27 dated tephra layers can be assigned to a specific planktonic foraminifer and nannofossil biozone, providing an age range within the adopted biochronology. The new radiometric ages display three types of relationships with respect to the biostratigraphic age ranges. In the majority of the analyzed tephra layers (15 examples), the weighted mean ^{40}Ar/^{39}Ar age lies within the narrowly defined biozone age range for each layer, as shown in Table 2. In most of the other samples the radiometric average age lies slightly outside the narrowly defined biozone age range (Table 2), even when the standard error is taken into account. In several cases, the weighted means are based on a large number of single-crystal analyses and with small error (e.g., Samples 165-999A-48X-6, 42–43 cm; 165-1000B-14R-2, 139–140 cm; 165-1000B-19R-2, 99–101 cm; and 165-998A-27X-1, 120–122 cm). In the majority of cases, these radiometric ages lie outside the designated age range of the planktonic foraminifer age estimates, but within the nannofossil age estimates. Further work is required to establish how close these tephra layers are to biozone boundaries, in order to utilize them to further constrain or tune the biochronostratigraphic time scale.

Biotite ages in three of the tephra layers are much older than indicated by the biochronology and the difference—tens of millions of years—is much greater than can be reasonably accounted for by errors in the current time scale (e.g., tephra layers in Samples 165-998A-13H-3, 32–33 cm; 165-1001A-36R-3, 70–71 cm; and 165-1001B-6R-3, 130–131 cm). There are several reasons why the ^{40}Ar/^{39}Ar ages might be much older. First, altered biotites tend to suffer from recoil more than less altered ones, and recoil loss of ^{39}Ar causes anomalously high ^{40}Ar*/^{39}Ar ratios and thus should produce higher apparent ages. All studies on altered biotites to date show, however, that alteration tends to decrease the apparent age (Adams and Kelley, 1997). Second, biotites may contain excess argon. This may include biotite grains that were in the magma chamber and experienced a high partial pressure of argon or took on mantle argon, but never fully degassed during the eruption. Third, the biotites may be xenocrysts, plucked from older wall rocks or conduit walls during or shortly be-

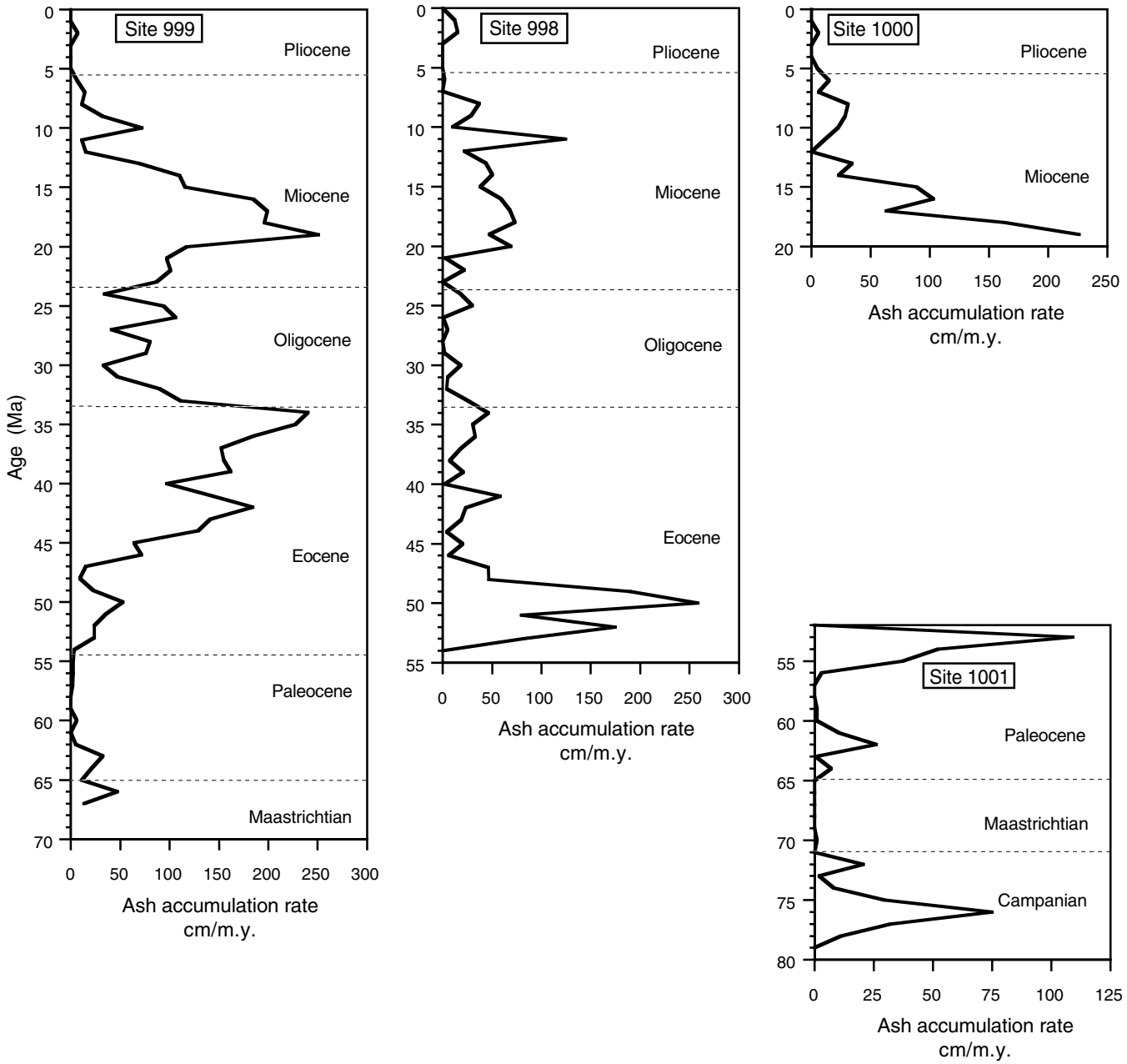

Figure 2. The accumulation rate of tephra layers at sites drilled during Leg 165, expressed as ash layer thickness (in centimeters per million years). Three major episodes are evident, the earliest in early Eocene (best shown at Sites 998 and 1001), late Eocene (Site 999), and Miocene (Sites 999 and 1000).

fore eruption and dispersed and deposited with the juvenile tephra. Finally, some of these high-age biotites may be in tephra layers that represent turbidites or other type of sediment from a terrigenous source, and thus not derived directly from a contemporaneous magmatic source.

Feldspar crystals were also separated from 16 tephra layers for $^{40}Ar/^{39}Ar$ dating. Upon analysis of these grains, it became clear that the majority were sodic plagioclase and thus with a potassium content too low for yielding meaningful dates. One layer contained common sanidine crystals, however, which provided 16 accurate single-crystal dates (Sample 165-999A-48X-6, 42–43 cm), with a weighted mean of 16.36 ± 0.31 Ma for the layer (Table 3). In comparison, the weighted mean age of six biotite crystals from the upper part of this layer (interval 165-999A-48X-6, 42–43 cm) is 17.98 ± 0.50 Ma. The difference in biotite and sanidine ages is significant, and may reflect slight alteration of the biotites.

TIMING, NATURE, AND SOURCE AREAS OF CARIBBEAN VOLCANISM

The results of drilling during Leg 165, with the recovery of thousands of tephra fall layers, volcaniclastic turbidites, and submarine basaltic lavas of the Caribbean oceanic crust, provide new insights into the timing and character of volcanism in the Caribbean region. The results are reviewed here in the context of the new dating and their implications with respect to the tectonic evolution of the region are discussed.

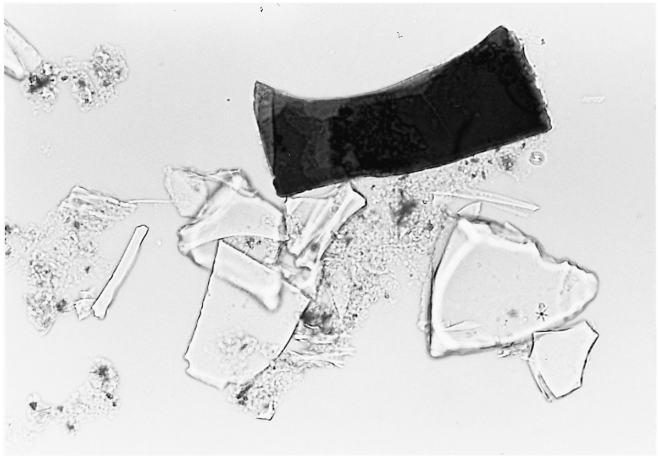

Figure 3. Photomicrograph of a biotite crystal (dark) and glass shards (clear) in Leg 165 tephra layer, of the type hand picked for $^{40}Ar/^{39}Ar$ dating (Sample 165-998A-19X-3, 55 cm. Width of field is ~0.5 mm.

Biochronology and Tephra Ages

With the discovery of numerous datable tephra layers in the sections cored at ODP Sites 998–1001, it was hoped that these Caribbean strata would provide a rare opportunity to test and refine the Cenozoic time scale. A revised Cenozoic geochronology and chronostratigraphy was recently published by Berggren et al. (1995a, 1995b). This time scale is based on a modified version of Cande and Kent's (1992, 1995) magnetochronology, which itself is based primarily on South Atlantic seafloor magnetic anomalies. Nine age calibration points, anchored by Chron C34n(y) at 83.0 Ma plus the zero-age ridge axis, and interpolated by a cubic spline function provide the numerical basis for the global polarity time scale. All calibration points are constrained directly by calcareous microfossil datums for purposes of correlation (Berggren et al., 1995b). The application of Milankovitch climate cyclicity to geochronology, corroborated by high precision $^{40}Ar/^{39}Ar$ dating, has provided a powerful tool in the effort to calibrate polarity boundaries and biostratigraphic datums in the younger part of the record (e.g., Shackleton et al., 1995a, 1995b). In their revised time scale, Berggren et al. (1995a, 1995b) accepted the astronomical time scale values of polarity events from the present to 5.23 Ma (Shackle-

Table 1: $^{40}Ar/^{39}Ar$ Dating of biotites from Leg 165 tephra layers.

Core, section, interval (cm)	Analysis number	$^{40}Ar/^{39}Ar$	$^{38}Ar/^{39}Ar$	$^{37}Ar/^{39}Ar$	$^{36}Ar/^{39}Ar$	^{39}Ar	Atm (%)	$^{40}Ar^*/^{39}Ar$	Age (Ma)	± (m.y.)	wi	xi*wi	Mean	Error
165-998A-														
13H-3, 32-33	1	12.497	0.172	0.000	0.016	49.28	61.11	7.636	40.73	0.98	1.04	42.4		
13H-3, 32-33	2	8.671	0.157	0.002	0.012	59.67	58.26	5.052	27.05	0.50	3.96	107.2		
13H-3, 32-33	3	4.431	0.163	0.015	0.001	20.92	90.63	4.016	21.53	0.99	1.02	22.1		
13H-3, 32-33	4	10.336	0.164	0.011	0.016	36.78	52.98	5.476	29.30	0.77	1.67	48.9		
13H-3, 32-33	5	16.674	0.175	0.024	0.031	17.42	44.86	7.480	39.91	1.29	0.60	24.1		
13H-3, 32-33	6	4.021	0.156	0.005	0.002	77.59	88.86	3.573	19.17	0.35	7.99	153.1		
													24.42	0.25
13H-5, 123-124	1	1.753	0.096	0.006	0.000	18.30	92.26	1.617	8.70	1.02	0.95	8.3		
13H-5, 123-124	2	1.401	0.101	–0.018	0.001	6.47	72.61	1.017	5.48	2.89	0.12	0.7		
13H-5, 123-124	3	1.721	0.097	–0.019	0.001	7.57	90.48	1.557	8.38	2.46	0.17	1.4		
13H-5, 123-124	4	1.317	0.100	–0.007	0.001	8.26	88.59	1.166	6.28	2.25	0.20	1.2		
13H-5, 123-124	5	1.314	0.090	–0.011	0.001	5.65	83.29	1.095	5.90	3.29	0.09	0.5		
													7.93	0.81
20X-1, 133-134	1	3.391	0.069	0.024	0.001	11.41	87.17	2.956	15.88	1.65	0.37	5.9		
20X-1, 133-134	2	2.703	0.069	0.012	0.000	17.76	94.83	2.564	13.78	1.06	0.89	12.2		
20X-1, 133-134	3	2.433	0.074	0.020	0.001	9.31	89.04	2.166	11.65	2.02	0.25	2.9		
													13.94	0.82
21X-4, 79-80	1	3.005	0.095	–0.001	0.001	9.97	91.71	2.756	14.81	1.88	0.28	4.2		
21X-4, 79-80	2	2.974	0.104	0.003	0.001	12.72	93.44	2.778	14.93	1.50	0.44	6.6		
21X-4, 79-80	3	2.869	0.099	0.009	0.001	8.71	90.07	2.584	13.88	2.13	0.22	3.0		
21X-4, 79-80	4	2.874	0.100	0.002	0.000	59.43	98.55	2.832	15.21	0.46	4.77	72.6		
21X-4, 79-80	5	3.308	0.103	0.001	0.001	15.99	95.31	3.153	16.93	1.25	0.64	10.9		
21X-4, 79-80	6	3.137	0.104	–0.020	0.001	8.61	90.80	2.848	15.30	2.19	0.21	3.2		
													15.30	0.39
27X-1, 120-122	1	3.802	0.120	–0.001	0.001	54.93	91.08	3.463	18.58	0.42	5.80	107.9		
27X-1, 120-122	2	3.274	0.130	–0.001	0.000	30.68	97.53	3.193	17.14	0.64	2.45	42.0		
27X-1, 120-122	3	3.247	0.127	0.001	0.000	41.87	96.35	3.129	16.80	0.50	4.03	67.7		
27X-1, 120-122	4	3.312	0.117	–0.002	0.000	34.53	97.83	3.241	17.40	0.59	2.88	50.1		
27X-1, 120-122	5	3.327	0.096	–0.001	0.000	18.88	96.05	3.195	17.15	1.05	0.91	15.7		
27X-1, 120-122	6	4.029	0.165	0.000	0.001	41.61	96.30	3.880	20.81	0.51	3.79	78.8		
27X-1, 120-122	7	3.671	0.141	–0.002	0.001	8.95	92.45	3.394	18.21	2.12	0.22	4.0		
27X-1, 120-122	8	3.544	0.103	–0.004	0.001	10.13	93.08	3.299	17.71	1.87	0.29	5.1		
27X-1, 120-122	9	3.482	0.147	0.003	0.001	27.85	93.60	3.259	17.50	0.75	1.78	31.1		
													18.16	0.21
29X-3, 68-69	1	5.191	0.159	–0.002	0.003	30.09	84.11	4.366	23.40	0.78	1.64	38.4		
29X-3, 68-69	2	4.689	0.160	–0.005	0.001	14.33	96.31	4.516	24.20	1.37	0.53	12.9		
29X-3, 68-69	3	4.129	0.160	0.000	0.000	50.96	98.82	4.080	21.87	0.52	3.65	79.8		
29X-3, 68-69	4	6.160	0.167	–0.004	0.005	39.09	73.72	4.541	24.33	0.72	1.94	47.2		
													22.97	0.36
29X-3, 69-70	1	2.343	0.059	0.016	0.001	19.69	86.55	2.028	10.90	0.95	1.10	12.0		
29X-3, 69-70	2	1.737	0.063	0.008	0.001	31.02	88.48	1.537	8.27	0.61	2.71	22.4		
29X-3, 69-70	3	19.636	0.095	0.021	0.040	29.02	39.45	7.746	41.31	1.41	0.50	20.7		
													12.79	0.48
52X-1, 128-129		5.555	0.116		0.000	0.0013	100.00	5.55	30.70	18.63			30.70	18.63
165-998B-														
1R-7, 53-54	1	6.095	0.103		0.000	0.0083	100.00	6.09	33.66	4.43	0.05	1.7		
1R-7, 53-54	2	6.141	0.215		0.003	0.0118	87.75	5.39	29.79	2.02	0.24	7.3		
1R-7, 53-54	3	6.258	0.233		0.000	0.0019	100.00	6.26	34.55	12.59	0.01	0.2		
1R-7, 53-54	4	6.571	0.076		0.000	0.0067	100.00	6.57	36.27	3.62	0.08	2.8		
1R-7, 53-54	5	5.931	0.080		0.001	0.0081	93.83	5.57	30.76	2.97	0.11	3.5		
1R-7, 53-54	6	8.236	0.198		0.008	0.0076	71.62	5.90	32.59	3.19	0.10	3.2		

Table 1 (continued).

Core, section, interval (cm)	Analysis number	$^{40}Ar/^{39}Ar$	$^{38}Ar/^{39}Ar$	$^{37}Ar/^{39}Ar$	$^{36}Ar/^{39}Ar$	^{39}Ar	Atm (%)	$^{40}Ar^*/^{39}Ar$	Age (Ma)	± (m.y.)	wi	xi*wi	Mean	Error
													31.67	1.30
165-999A-														
27X-2, 150	1	0.873	0.0135	0.0001	0.000323967	156.999	89.03	0.7770	8.32	0.38	6.90	57.4		
27X-2, 150	2	0.862	0.0131	0.0037	0.000219742	135.332	92.46	0.7968	8.53	0.44	5.13	43.8		
27X-2, 150	3	0.908	0.0135	0.0106	0.000140563	149.829	95.42	0.8663	9.28	0.40	6.27	58.2		
27X-2, 150	4	0.913	0.0146	0.0229	0.000477364	113.962	84.55	0.7721	8.27	0.52	3.65	30.2		
27X-2, 150	5	0.890	0.0138	0.0153	0.000720032	35.454	76.09	0.6770	7.25	1.68	0.36	2.6		
27X-2, 150	6	0.841	0.0146	0.0095	0.0000	37.418	100.00	0.8411	9.01	1.59	0.40	3.6		
27X-2, 150	7	0.870	0.0142	0.0028	0.000772052	33.214	73.79	0.6423	6.88	1.79	0.31	2.1		
27X-2, 150	8	0.858	0.0129	0.0004	0.000654051	45.658	77.47	0.6645	7.12	1.30	0.59	4.2		
27X-2, 150	9	0.906	0.0130	0.0201	0.000502838	100.138	83.59	0.7571	8.11	0.59	2.83	22.9		
27X-2, 150	10	0.954	0.0149	0.0154	0.000657564	76.896	79.64	0.7599	8.14	0.77	1.67	13.6		
27X-2, 150	11	0.918	0.0130	0.0121	0.0000	84.521	100.00	0.9176	9.82	0.69	2.11	20.7		
27X-2, 150	12	0.892	0.0151	0.0302	0.000108367	30.152	96.41	0.8603	9.21	1.93	0.27	2.5		
27X-2, 150	13	0.925	0.0139	0.0239	0.000621899	59.078	80.14	0.7416	7.94	0.98	1.03	8.2		
27X-2, 150	14	0.871	0.0137	0.0116	0.000753646	49.035	74.43	0.6481	6.94	1.19	0.71	4.9		
27X-2, 150	15	0.918	0.0136	0.0145	0.000399538	81.591	87.14	0.8001	8.57	0.71	1.97	16.8		
27X-2, 150	16	1.041	0.0139	0.0118	0.000783483	41.832	77.75	0.8090	8.66	1.39	0.52	4.5		
27X-2, 150	17	0.900	0.0136	0.0068	0.000538336	84.250	82.33	0.7413	7.94	0.69	2.10	16.6		
													8.50	0.16
28X-5, 13-14	1	1.525	0.061		0.000	0.0034	100.00	1.53	8.48	6.97	0.02	0.2		
28X-5, 13-14	2	1.701	0.059		0.000	0.0035	100.00	1.70	9.46	6.80	0.02	0.2		
28X-5, 13-14	3	1.905	0.058		0.000	0.0023	100.00	1.91	10.59	10.16	0.01	0.1		
28X-5, 13-14	4	0.538	0.056		0.000	0.0013	100.00	0.54	2.99	17.98	0.00	0.0		
													8.93	4.26
40X-1, 57-58	1	3.270	0.062		0.002	0.0066	86.29	2.82	15.66	3.59	0.08	1.2		
40X-1, 57-58	2	3.207	0.061		0.000	0.0039	100.00	3.21	17.79	6.06	0.03	0.5		
40X-1, 57-58	3	3.077	0.059		0.000	0.0009	100.00	3.08	17.07	25.66	0.00	0.0		
													16.23	3.07
41X-4, 41-42	1	3.365	0.099		0.000	0.0055	100.00	3.37	18.66	4.29	0.05	1.0		
41X-4, 41-42	2	4.025	0.101		0.000	0.0037	100.00	4.02	22.30	6.44	0.02	0.5		
41X-4, 41-42	3	3.504	0.100		0.000	0.0033	100.00	3.50	19.43	7.15	0.02	0.4		
41X-4, 41-42	4	4.380	0.121		0.009	0.0023	41.20	1.80	10.03	16.09	0.00	0.0		
41X-4, 41-42	5	3.651	0.098		0.000	0.0021	100.00	3.65	20.24	17.49	0.00	0.1		
41X-4, 41-42	6	3.840	0.096		0.000	0.0031	100.00	3.84	21.28	7.55	0.02	0.4		
41X-4, 41-42	7	4.091	0.076		0.003	0.0033	77.78	3.18	17.65	7.25	0.02	0.3		
													19.38	2.66
45X-2, 94-95	1	4.137	0.079		0.003	0.0034	78.89	3.26	18.11	6.96	0.02	0.4		
45X-2, 94-95	2	4.366	0.076		0.001	0.0070	90.33	3.94	21.85	3.37	0.09	1.9		
45X-2, 94-95	3	4.579	0.072		0.005	0.0020	68.17	3.12	17.32	11.62	0.01	0.1		
45X-2, 94-95	4	4.082	0.086		0.004	0.0023	68.45	2.79	15.51	10.27	0.01	0.1		
45X-2, 94-95	5	2.815	0.058		0.003	0.0031	65.64	1.85	10.27	7.73	0.02	0.2		
													19.29	2.65
48X-6, 42-43	1	3.936	0.091		0.003	0.0188	76.05	2.99	16.61	1.27	0.62	10.3		
48X-6, 42-43	2	3.899	0.080		0.002	0.0316	85.61	3.34	18.51	0.78	1.65	30.6		
48X-6, 42-43	3	3.270	0.085		0.001	0.0165	89.07	2.91	16.17	1.45	0.47	7.7		
48X-6, 42-43	4	3.664	0.077		0.002	0.0131	87.67	3.21	17.82	1.83	0.30	5.3		
48X-6, 42-43	5	3.873	0.085		0.002	0.0250	87.78	3.40	18.85	1.00	1.01	19.0		
													17.98	0.50
165-999B-														
7R-CC, 13-14	1	6.865	0.123		0.008	0.0024	64.63	4.44	24.56	9.67	0.01	0.3		
7R-CC, 13-14	2	3.354	0.091		0.000	0.0019	100.00	3.35	18.60	12.15	0.01	0.1		
7R-CC, 13-14	3	5.232	0.182		0.003	0.0116	80.53	4.21	23.34	2.05	0.24	5.6		
7R-CC, 13-14	4	5.558	0.205		0.004	0.0044	76.08	4.23	23.42	5.29	0.04	0.8		
7R-CC, 13-14	5	4.611	0.070		0.000	0.0054	100.00	4.61	25.52	6.77	0.02	0.6		
													23.44	1.79
15R-2, 45-46	1	5.253	0.117		0.000	0.0042	100.00	5.25	29.05	5.58	0.03	0.9		
15R-2, 45-46	2	5.415	0.110		0.002	0.0059	90.67	4.91	27.17	4.02	0.06	1.7		
15R-2, 45-46	3	5.754	0.126		0.002	0.0189	91.84	5.28	29.22	1.39	0.51	15.0		
15R-2, 45-46	4	4.982	0.111		0.002	0.0046	87.15	4.34	24.04	5.09	0.04	0.9		
15R-2, 45-46	5	5.150	0.111		0.003	0.0116	85.19	4.39	24.29	2.04	0.24	5.8		
15R-2, 45-46	6	5.150	0.112		0.000	0.0075	100.00	5.15	28.49	3.13	0.10	2.9		
15R-2, 45-46	7	5.150	0.113		0.000	0.0124	100.00	5.15	28.48	1.44	0.48	13.7		
15R-2, 45-46	8	4.940	0.119		0.004	0.0089	73.25	3.62	20.06	2.65	0.14	2.8		
													27.21	0.79
47R-6, 4-5	1	16.275	0.057		0.000	0.0006	100.00	16.27	88.52	38.59	0.00	0.1		
47R-6, 4-5	2	10.245	0.040		0.005	0.0037	84.33	8.64	47.53	6.34	0.02	1.2		
													48.61	1.15
48R-3, 6-7	1	10.377	0.109		0.002	0.0048	94.07	9.76	53.62	4.94	0.04	2.2		
48R-3, 6-7	2	9.351	0.106		0.000	0.0091	100.00	9.35	51.39	2.71	0.14	7.0		
48R-3, 6-7	3	9.728	0.107		0.000	0.0081	100.00	9.73	53.43	4.49	0.05	2.7		
48R-3, 6-7	4	9.686	0.101		0.000	0.0039	100.00	9.69	53.20	6.12	0.03	1.4		
48R-3, 6-7	5	9.149	0.106		0.000	0.0036	100.00	9.15	50.29	6.48	0.02	1.2		
48R-3, 6-7	6	9.744	0.111		0.002	0.0042	92.86	9.05	49.75	8.52	0.01	0.7		
48R-3, 6-7	7	10.040	0.107		0.000	0.0031	100.00	10.04	55.12	7.61	0.02	1.0		
48R-3, 6-7	8	14.070	0.104		0.014	0.0035	70.41	9.91	54.40	6.56	0.02	1.3		
48R-3, 6-7	9	9.966	0.099		0.001	0.0190	96.88	9.66	53.04	1.67	0.36	19.0		
48R-3, 6-7	10	9.473	0.101		0.003	0.0034	90.75	8.60	47.30	6.99	0.02	1.0		
48R-3, 6-7	11	9.832	0.108		0.000	0.0103	100.00	9.83	54.00	2.64	0.14	7.7		
48R-3, 6-7	12	9.429	0.108		0.000	0.0048	100.00	9.43	51.81	5.07	0.04	2.0		
48R-3, 6-7	13	12.003	0.101		0.000	0.0047	100.00	12.00	65.70	5.35	0.03	2.3		
48R-3, 6-7	14	9.617	0.101		0.001	0.0075	95.90	9.22	50.69	3.23	0.10	4.9		
48R-3, 6-7	15	10.489	0.099		0.004	0.0023	87.72	9.20	50.58	10.15	0.01	0.5		
48R-3, 6-7	16	9.607	0.089		0.005	0.0021	85.35	8.20	45.14	11.66	0.01	0.3		

Table 1 (continued).

Core, section, interval (cm)	Analysis number	$^{40}Ar/^{39}Ar$	$^{38}Ar/^{39}Ar$	$^{37}Ar/^{39}Ar$	$^{36}Ar/^{39}Ar$	^{39}Ar	Atm (%)	$^{40}Ar^*/^{39}Ar$	Age (Ma)	± (m.y.)	wi	xi*wi	Mean	Error
48R-3, 6-7	17	10.351	0.101		0.003	0.0063	90.96	9.42	51.74	3.73	0.07	3.7		
48R-3, 6-7	18	9.030	0.096		0.004	0.0048	86.37	7.80	42.96	4.90	0.04	1.8		
48R-3, 6-7	19	9.706	0.089		0.000	0.0028	100.00	9.71	53.31	8.43	0.01	0.7		
48R-3, 6-7	20	8.934	0.086		0.000	0.0026	100.00	8.93	49.13	8.86	0.01	0.6		
													52.47	0.92
165-1000A-														
16H-6, 21-22	1	2.252	0.104	–0.002	0.002	32.38	74.48	1.678	8.94	0.86	1.35	12.0		
16H-6, 21-22	2	2.028	0.088	–0.001	0.005	48.24	30.22	0.613	3.27	0.43	5.30	17.3		
16H-6, 21-22	3	3.424	0.096	–0.003	0.002	12.55	82.67	2.83	15.05	1.55	0.41	6.2		
16H-6, 21-22	4	2.071	0.103	0.001	0.004	50.05	36.53	0.756	4.04	0.38	6.83	27.6		
16H-6, 21-22	5	1.362	0.096	–0.003	0.000	29.81	93.89	1.279	6.82	0.68	2.18	14.9		
16H-6, 21-22	6	0.884	0.100	0.000	0.000	19.37	85.51	0.756	4.03	0.98	1.04	4.2		
													4.80	0.24
28H-1, 88-89	1	1.382	0.083	0.006	0.000	66.03	94.56	1.307	6.96	0.30	11.05	77.0		
28H-1, 88-89	2	1.452	0.088	0.006	0.000	64.36	94.69	1.375	7.33	0.30	11.41	83.6		
28H-1, 88-89	3	1.591	0.089	0.006	0.000	63.82	95.11	1.513	8.06	0.32	9.72	78.4		
28H-1, 88-89	4	1.364	0.085	0.027	0.001	18.03	69.71	0.950	5.07	1.03	0.95	4.8		
28H-1, 88-89	5	1.565	0.082	0.002	0.000	66.53	97.62	1.528	8.14	0.44	5.07	41.3		
													7.46	0.16
165-1000B-														
14R-2, 139-140	1	3.695	0.107	0.011	0.001	27.20	95.06	3.512	18.66	0.76	1.73	32.2		
14R-2, 139-140	2	3.471	0.100	0.000	0.000	25.02	97.14	3.371	17.91	0.80	1.57	28.1		
14R-2, 139-140	3	4.342	0.108	0.007	0.004	15.87	72.99	3.169	16.85	1.21	0.69	11.6		
14R-2, 139-140	4	3.634	0.109	0.006	0.000	33.85	97.98	3.561	18.92	0.69	2.12	40.2		
14R-2, 139-140	5	3.555	0.112	0.006	0.000	29.38	97.62	3.470	18.44	0.72	1.92	35.4		
14R-2, 139-140	6	3.451	0.095	0.004	0.000	29.10	97.53	3.366	17.89	0.89	1.26	22.5		
													18.31	0.33
16R-5, 84-85	1	3.391	0.108	–0.002	0.000	57.97	98.74	3.348	17.79	0.53	3.59	63.9		
16R-5, 84-85	2	3.583	0.078	0.000	0.000	50.61	98.63	3.534	18.77	0.48	4.37	82.1		
16R-5, 84-85	3	3.546	0.090	0.001	0.000	62.65	98.88	3.506	18.63	0.43	5.53	103.1		
16R-5, 84-85	4	3.357	0.088	0.001	0.000	115.30	99.36	3.336	17.73	0.75	1.77	31.3		
16R-5, 84-85	5	3.196	0.163	0.002	0.000	74.19	98.95	3.162	16.81	0.35	8.15	136.9		
16R-5, 84-85	6	3.256	0.082	0.002	0.000	76.82	99.01	3.224	17.14	0.33	9.39	161.0		
16R-5, 84-85	7	3.212	0.108	0.002	0.000	100.83	99.23	3.188	16.94	0.93	1.14	19.4		
16R-5, 84-85	8	3.282	0.095	0.005	0.000	61.53	98.77	3.241	17.23	0.35	8.29	142.7		
16R-5, 84-85	9	3.300	0.103	0.008	0.000	37.29	97.98	3.233	17.18	0.52	3.71	63.7		
													17.50	0.15
19R-2, 99-101	1	3.284	0.209	0.007	0.000	55.55	98.64	3.239	17.22	0.74	1.81	31.2		
19R-2, 99-101	2	3.088	0.211	0.009	0.000	35.90	97.76	3.019	16.05	0.67	2.20	35.4		
19R-2, 99-101	3	3.443	0.223	0.005	0.000	42.97	98.32	3.385	17.99	0.48	4.38	78.8		
19R-2, 99-101	4	3.152	0.219	0.016	0.000	20.34	96.13	3.030	16.11	0.97	1.06	17.0		
19R-2, 99-101	5	3.184	0.219	0.007	0.000	38.88	97.99	3.120	16.59	0.60	2.73	45.3		
19R-2, 99-101	6	3.534	0.213	–0.002	0.000	49.66	98.59	3.484	18.51	0.50	3.95	73.1		
19R-2, 99-101	7	3.557	0.218	0.001	0.000	42.45	98.36	3.499	18.59	0.86	1.35	25.2		
19R-2, 99-101	8	3.459	0.211	0.008	0.000	33.95	97.89	3.386	17.99	0.65	2.40	43.2		
19R-2, 99-101	9	3.665	0.217	0.003	0.005	44.68	62.11	2.28	12.12	0.44	5.14	62.2		
19R-2, 99-101	10	3.520	0.211	0.001	0.000	114.99	99.39	3.498	18.59	0.55	3.25	60.5		
19R-2, 99-101	11	3.320	0.212	0.002	0.000	92.22	99.19	3.293	17.50	0.68	2.19	38.4		
19R-2, 99-101	12	3.618	0.219	0.003	0.000	75.98	99.10	3.586	19.05	0.76	1.73	33.0		
19R-2, 99-101	13	3.629	0.209	0.001	0.000	91.31	99.25	3.602	19.13	0.66	2.27	43.5		
													17.02	0.17
165-1001A-														
26R-2, 63-64	1	12.237	0.078	–0.018	0.001	7.62	97.34	11.911	62.51	3.12	0.10	6.4		
26R-2, 63-64	2	12.007	0.079	–0.008	0.002	15.63	96.03	11.530	60.55	1.98	0.25	15.4		
26R-2, 63-64	3	10.605	0.085	0.009	0.002	4.30	94.56	10.028	52.77	4.59	0.05	2.5		
													60.14	1.57
36R-3, 70-71	1	21.041	0.094	–0.008	0.015	12.24	78.31	16.48	85.91	3.01	0.11	9.5		
36R-3, 70-71	2	19.788	0.104	–0.001	0.016	27.33	75.67	14.974	78.24	2.25	0.20	15.5		
36R-3, 70-71	3	23.395	0.120	–0.001	0.028	11.63	64.42	15.072	78.74	2.51	0.16	12.5		
36R-3, 70-71	4	20.707	0.108	0.008	0.016	22.07	77.19	15.983	83.39	1.95	0.26	21.8		
36R-3, 70-71	5	19.749	0.100	0.017	0.017	14.72	73.96	14.607	76.36	1.76	0.32	24.7		
36R-3, 70-71	6	16.086	0.119	0.018	0.012	12.90	77.27	12.429	65.18	2.00	0.25	16.2		
36R-3, 70-71	7	19.251	0.119	0.025	0.016	12.76	75.74	14.582	76.23	2.29	0.19	14.5		
36R-3, 70-71	8	16.926	0.091	0.009	0.012	39.39	79.71	13.492	70.65	1.14	0.77	54.7		
													74.78	0.66
165-1001B-														
6R-3, 130-131	1	15.762	0.192	0.024	0.001	6.28	97.49	15.366	80.25	3.45	0.08	6.8		
6R-3, 130-131	2	16.520	0.189	0.058	0.002	3.88	96.13	15.880	82.87	5.22	0.04	3.0		
													81.04	2.88

Notes: %Atm = 100*[($^{40}Ar/^{39}Ar$-295.5*$^{36}Ar/^{39}Ar$)/$^{40}Ar/^{39}Ar$]. $^{40}Ar^*/^{39}Ar$ = the ratio of the radiogenic isotope of argon (^{40}Ar) to the ^{39}Ar produced in the reactor from potassium. wi = the weighting used in the weighted mean and is the inverse of variance on each measurement. xi*wi = the weighting multiplied by the measured age of each measurement.

Table 2. Comparison of Leg 165 $^{40}Ar/^{39}Ar$ radiometric dates of tephra layers vs. biostratigraphic ages.

Leg, hole, core, section, interval (cm)	Tephra layer		Biostratigraphic datum ranges			Source of biostratigraphy	Biostratigraphic age (Ma)	Tephra			
	Number of grains	Depth (mbsf)	Age model	Interpolated depth (mbsf)	Age (Ma)			Age (Ma)	Error (Ma)	Age range (Ma)	Rank
165-1000A-16H-6, 21-22	6	144.01	1	120.05-148.55	3.80-4.37	Nannofossils: 1	4.28	**4.80**	**0.24**	**4.56-5.04**	**1**
			2, 3	120.05-148.55	3.82-4.8	Nannofossils: 1	**4.64**				
			2, 4	120.05-148.55	3.82-4.56	Nannofossils: 1	4.44				
165-998A-13H-3, 32-33	6	116.62	1	113.90-116.85	6.50-7.24	Nannofossils: 1	7.18	*24.42*	*0.25*	*24.17-24.67*	**4**
			2	113.90-116.85	6.76-7.39	Nannofossils: 1	7.34				
			5	113.90-116.85	6.84-7.39	Nannofossils: 1	7.35				
			7	113.00-121.20	5.875-6.555	Paleomagnetism 3*	6.18				
			7	110.05-122.40	5.230-6.919	Paleomagnetism 3*	6.13				
165-998A-13H-5, 123-124	5	120.53	1	116.85-126.40	7.24-7.80	Nannofossils: 1	**7.46**	**7.93**	**0.81**	**7.12-8.74**	**2**
			2, 4	116.85-126.40	7.39-7.73	Nannofossils: 1	**7.52**				
			7	113.00-121.20	5.875-6.555	Paleomagnetism 3*	6.50				
			7	110.05-122.40	5.230-6.919	Paleomagnetism 3*	6.66				
165-1000A-28H-1, 88-89	5	251.18	1	250.55-286.05	7.24-8.35	Nannofossils: 1	7.26	**7.46**	**0.16**	**7.30-7.62**	**1**
			2	250.55-286.05	7.39-8.20	Nannofossils: 1	**7.40**				
165-999A-27X-2, 150	17	242.10	1	231.61-245.71	8.35-8.43	Nannofossils: 1	**8.41**	**8.50**	**0.16**	**8.34-8.66**	**1**
			2, 1	231.61-245.71	8.20-8.43	Nannofossils: 1	**8.37**				
			3	231.61-245.71	8.6-8.7	Nannofossils: 1	8.67				
			6	237.54-265.56	8.58-9.82	Foraminifers: 2	8.78				
			3	237.54-265.56	8.3-10.9	Foraminifers: 2	8.68				
			6	237.54-269.11	8.58-10.49	Foraminifers: 2	8.86				
			3	237.54-269.11	8.3-11.4	Foraminifers: 2	8.75				
165-999A-28X-5, 13-14	4	254.83	1	245.71-257.17	8.43-9.43	Nannofossils: 1	**9.23**	8.93	4.26	4.67-13.19	**3**
			4	245.71-257.17	8.45-9.37	Nannofossils: 1	**9.18**				
			6	237.54-265.56	8.58-9.82	Foraminifers: 2	**9.26**				
			3	237.54-265.56	8.3-10.9	Foraminifers: 2	**9.72**				
			6	237.54 -269.11	8.58-10.49	Foraminifers: 2	**9.63**				
			3	237.54-269.11	8.3-11.4	Foraminifers: 2	**10.00**				
		Chron C5n.1n (o)		254.58-257.35		Paleomagnetism 3*	**9.78**				
165-998A-20X-1, 133-134	3	177.23	1	172.70-195.44	13.57-15.83	Nannofossils: 1	**14.02**	**13.94**	**0.82**	13.12-14.76	**2**
			3	172.70-195.44	13.6-15.6	Nannofossils: 1	**14.00**				
165-998A-21X-4, 79-80	6	190.79	1	172.70-195.44	13.57-15.83	Nannofossils: 1	**15.37**	**15.30**	**0.39**	**14.91-15.69**	**1**
			3	172.70-195.44	13.6-15.6	Nannofossils: 1	**15.19**				
165-999A-40X-1, 57-58	3	364.57	1	363.85-451.30	15.83-18.10	Nannofossils: 1	**15.85**	16.23	3.07	13.16-19.30	**3**
			3	363.85-451.30	15.6-18.2	Nannofossils: 1	**15.62**				
			3	345.75-416.25	14.8-16.4	Foraminifers: 2	**15.23**				
165-999A-41X-4, 41-42	7	378.61	1	363.85-451.30	15.83-18.10	Nannofossils: 1	16.21	19.38	2.66	16.72-22.04	**3?**
			3	363.85-451.30	15.6-18.2	Nannofossils: 1	16.04				
			3	345.75 -416.25	14.8-16.4	Foraminifers: 2	15.55				
165-999A-45X-2, 94-95	5	414.54	1	363.85-451.30	15.83-18.10	Nannofossils: 1	**17.15**	19.29	2.65	16.64-21.94	**3?**
			3	363.85-451.30	15.6-18.2	Nannofossils: 1	**17.11**				
			3	345.75-416.25	14.8-16.4	Foraminifers: 2	16.36				
165-999A-48X-6, 42-43	6	449.02	1	363.85-451.30	15.83-18.10	Nannofossils: 1	**18.04**	**17.98**	**0.5**	**17.48-18.48**	**1**
			3	363.85-451.30	15.6-18.2	Nannofossils: 1	**18.13**				
			3	416.25-454.14	16.4-17.3	Foraminifers: 2	17.18				
165-999A-48X-6, 42-43 (sanidine)	16							*16.36*	*0.31*	*16.05-16.67*	**3?**
165-1000B-14R-2, 139-140	6	611.77	1	557.35-643.30	15.83-18.1	Nannofossils: 3*	17.27	18.31	0.33	17.98-18.64	**3?**
			3	557.35-643.30	15.6-18.2	Nannofossils: 3*	17.25				
			3	590.05-633.40	16.4-17.3	Foraminifers: 3	16.85				
165-1000B-16R-5, 84-85	9	635.44	1	557.35-643.30	15.83-18.1	Nannofossils: 3*	17.89	17.50	0.15	17.35-17.65	**1?**
			3	557.35-643.30	15.6-18.2	Nannofossils: 3*	17.96				
165-1000B-19R-2, 99-101	13	659.89	1	643.30-668.90	18.1-19.7	Nannofossils: 3*	19.14	17.02	0.17	16.85-17.19	**3?**
			3	643.30-668.90	18.2-19.2	Nannofossils: 3*	18.85				
165-998A-27X-1, 120-122	8	244.40	1	242.56-244.95	18.10-18.40	Nannofossils: 1	**18.33**	18.16	0.21	17.95-18.37	**1**
			3	242.56-244.95	18.2-18.3	Nannofossils: 1	**18.28**				
165-998A-29X-3, 68-69	4	266.18	1	257.65-330.01	19.70-23.80	Nannofossils: 1	20.18	22.97	0.36	22.61-23.33	**3?**
			3	257.65-330.01	19.2-23.8	Nannofossils: 1	19.74				
165-998A-29X-3, 68-69	3							*12.79*	*0.48*		**4**
165-999B-7R-CC, 13-14	5	591.70	3	480.10-605.96	19.2-23.8	Nannofossils: 3*	**23.28**	**23.44**	**1.79**	21.65-25.23	**3**
			3	454.38-605.96	17.3-23.8	Foraminifers: 3	**23.19**				
165-999B-15R-2, 45-46	8	661.05	3	654.42-680.26	27.5-29.9	Nannofossils: 3*	28.12	**27.21**	**0.79**	**26.42-28.00**	**2?**
			3	605.96-710.92	23.8-32.0	Foraminifers: 3	28.10				
165-998A-52X-1, 128-129	1	484.98	3	448.39-486.98	27.5-29.9	Nannofossils: 3*	29.78	**30.70**	**18.60**	12.1-49.3	**3**
			3	448.39-514.25	27.5-31.5	Nannofossils: 3*	29.72				
			3	443.81-494.47	27.1-28.5	Foraminifers: 3	28.20				
165-998B-1R-7, 53-54	6	567.30	3	566.95-576.55	32.3-32.8	Nannofossils: 3*	**32.32**	**31.67**	**1.30**	30.37-32.97	**2**
			3	514.25-586.00	31.5-34.2	Nannofossils: 3*	33.50				
165-999B-47R-6, 4-5	2	937.54	3	918.44-949.89	49.7-52.85	Nannofossils: 3*	51.61	48.61	1.15	47.46-49.76	**3?**
			3	864.39-949.89	46.1-52.85	Nannofossils: 3*	51.87				
			3	843.60-951.84	43.6-52.3	Foraminifers: 3	51.15				
165-999B-48R-3, 6-7	20	942.66	3	918.44-949.89	49.7-52.85	Nannofossils: 3*	**52.13**	**52.47**	**0.92**	**51.55-53.39**	**2**
			3	864.39-949.89	46.1-52.85	Nannofossils: 3*	**52.28**				
			3	843.60-951.84	43.6-52.3	Foraminifers: 3	**51.56**				
165-1001A-26R-2, 63-64	3	229.93	3	169.89-234.10	52.85-55.3	Nannofossils: 3*	55.14	*60.14*	*1.57*	*58.57-61.71*	**3?(4?)**
			3	169.89-267.79	52.85-56.2	Nannofossils: 3*	54.90				
			7	204.20-259.50	53.347-55.904	Paleomagnetism 3*	54.54				
165-1001B-6R-3, 130-131	2	238.90	3	232.31-262.29	55.3-56.2	Nannofossils: 3*	55.50	*81.04*	*2.88*	*78.16-83.92*	**4**
			3	232.31-285.94	55.3-57.5	Nannofossils: 3*	55.57				

Table 2 (continued).

Leg, hole, core, section, interval (cm)	Tephra layer: Number of grains	Tephra layer: Depth (mbsf)	Biostratigraphic datum ranges: Age model	Biostratigraphic datum ranges: Interpolated depth (mbsf)	Biostratigraphic datum ranges: Age (Ma)	Source of biostratigraphy	Biostratigraphic age (Ma)	Tephra: Age (Ma)	Tephra: Error (Ma)	Tephra: Age range (Ma)	Rank
			7	204.20-259.50	53.347-55.904	Paleomagnetism 3*	54.95				
165-1001A-36R-3, 70-71	8	327.50	3	296.77-327.63	58.4-59.7	Nannofossils: 3*	59.69	*74.78*	*0.66*	*74.12-75.44*	4
			7	291.90-331.35	57.911-60.920	Paleomagnetism 3*	60.63				

Notes: Age model: 1 = ages of Kameo and Bralower (Chap. 1, this volume), includes ages of Raffi and Flores (1995) for interval 5–17 Ma; 2 = ages of I. Raffi (unpubl. data, 1999); 3 = ages of Berggren et al. (1995a, 1995b); 4 = ages of Shackleton et al. (1995); 5 = ages of Backman and Raffi (1997); 6 = ages of Chaisson and Pearson (1997) and Pearson and Chaisson (1997); and 7 = magnetochron ages as summarized in Sigurdsson, Leckie, Acton, et al. (1997). Biostratigraphic sources: 1 = high-resolution calcareous nannofossil biostratigraphy of Holes 998A, 999A, and 1000A from Kameo and Bralower (Chap. 1, this volume); 2 = high-resolution planktonic foraminiferal biostratigraphy of Hole 999A from Chaisson and D'Hondt (Chap. 2, this volume); 3 = low- to high(*)-resolution shipboard biostratigraphy and paleomagnetism from Sigurdsson, Leckie, Acton, et al. (1997); 4 = this study; and boldface = within error. Tephra rank: 1 = congruent age with small error (<0.5 m.y.); 2 = congruent age with larger error (0.5-1.5 m.y.); 3 = reasonable mean but very large error (>1.5 m.y.), or suspect age; 4 = incongruent age (diagenetic alteration or sedimentary reworking); boldface = radiometric ages in good agreement with biostratigraphy and with small errors; and italics = radiometric ages from diagenetically altered or reworked mineral grains.

Table 3: $^{40}Ar/^{39}Ar$ Dating of feldspars in Leg 165 tephra layer.

Core, section, interval (cm)	Analysis number	$^{40}Ar/^{39}Ar$	$^{38}Ar/^{39}Ar$	$^{37}Ar/^{39}Ar$	$^{36}Ar/^{39}Ar$	^{39}Ar	$^{40}Ar^*$ (%)	$^{40}Ar^*/^{39}Ar$	Age (Ma)	± (m.y.)	wi	xi*wi	Mean (Ma)	Error (Ma)
165-999A-														
48X-6, 43	1	1.80	0.013	1.62	0.0010	16.3	84.36	1.516	16.21	3.17	0.10	1.62		
48X-6, 43	2	1.77	0.012	1.43	0.0016	20.2	73.72	1.302	13.93	2.56	0.15	2.12		
48X-6, 43	3	1.69	0.012	0.59	0.0006	23.3	89.06	1.504	16.08	2.22	0.20	3.27		
48X-6, 43	4	2.11	0.013	0.77	0.0009	36.4	87.75	1.854	19.79	1.42	0.49	9.79		
48X-6, 43	5	1.75	0.013	0.96	0.0000	38.0	99.85	1.743	18.62	1.36	0.54	10.07		
48X-6, 43	6	1.69	0.012	0.81	0.0000	33.9	100.00	1.693	18.08	1.53	0.43	7.77		
48X-6, 43	7	1.82	0.014	1.09	0.0013	32.6	78.82	1.436	15.35	1.59	0.40	6.10		
48X-6, 43	8	1.81	0.012	1.73	0.0013	32.7	79.26	1.431	15.30	1.58	0.40	6.10		
48X-6, 43	9	1.83	0.010	1.84	0.0016	22.8	74.08	1.359	14.53	2.26	0.20	2.83		
48X-6, 43	10	1.88	0.014	0.71	0.0008	39.5	87.42	1.644	17.57	1.10	0.83	14.60		
48X-6, 43	11	2.00	0.017	0.05	0.0024	12.9	65.23	1.304	13.94	3.36	0.09	1.23		
48X-6, 43	12	2.08	0.017	0.43	0.0012	23.4	83.12	1.730	18.47	1.85	0.29	5.42		
48X-6, 43	13	2.31	0.014	0.57	0.0033	40.2	57.48	1.329	14.21	1.08	0.86	12.16		
48X-6, 43	14	1.96	0.015	0.27	0.0014	81.8	78.37	1.535	16.40	0.54	3.47	56.96		
48X-6, 43	15	1.91	0.021	0.38	0.0014	31.5	78.30	1.497	16.00	1.38	0.53	8.46		
48X-6, 43	16	2.15	0.015	0.28	0.0024	52.4	66.58	1.432	15.30	0.83	1.45	22.26		
													16.36	0.31

Notes: %Atm = 100*[($^{40}Ar/^{39}Ar$-295.5*$^{36}Ar/^{39}Ar$)$^{40}Ar/Ar$]. $^{40}Ar^*/^{39}Ar$ = the ratio of the radiogenic isotope of argon (^{40}Ar) to the ^{39}Ar produced in the reactor from potassium. wi = the weighting used in the weighted mean and is the inverse of variance on each measurement. xi*wi = the weighting multiplied by the measured age of each measurement.

ton et al., 1990; Hilgen, 1991; Langereis et al., 1994). The magnetic polarity time scale used for ODP Leg 165 adopted the astronomically tuned time scale of Shackleton et al. (1995b) and Shackleton and Crowhurst (1997) for the interval from 5 to 14 Ma (Sigurdsson, Leckie, Acton, et al., 1997).

Astronomical calibration of calcareous nannofossil and planktonic foraminiferal first and last occurrences (FO and LO) has been applied back to at least 13.5 Ma (Shackleton et al., 1995a; Raffi and Flores, 1995; Berggren et al., 1995a; Backman and Raffi, 1997; Chaisson and Pearson, 1997; Pearson and Chaisson, 1997); biostratigraphic datums older than 13.5 Ma are from Berggren et al., (1995b, appendices 1 and 2). It is within this framework that we compare the ages of the dated tephra levels based on biostratigraphy to the $^{40}Ar/^{39}Ar$ ages of the individual tephras (Fig. 4). We present several biostratigraphic age estimates for each of the tephra layers based on one or more pairs of calcareous nannofossil and planktonic foraminiferal datums, and/or different age models for these biostratigraphic datum pairs (Table 2). We ranked the tephra $^{40}Ar/^{39}Ar$ ages according to magnitude of analytical error and relative congruence with the biostratigraphic age: 1 = congruent age with small error (<0.5 Ma); 2 = congruent age with larger error (0.5–1.5 Ma); 3 = reasonably congruent mean but very large error (>1.5 Ma), or suspect (incongruent?) age; and 4 = an incongruent age because of diagenetic alteration or sedimentary reworking.

Our findings demonstrate that there is excellent agreement between the astrochronologically tuned nannofossil ages and the radiometric ages of the tephra layers for the interval from 4.8 to 15.3 Ma; the interpolated planktonic foraminiferal ages yield less congruent ages (Fig. 4). Strata older than the early middle Miocene yield mixed results. Some of the radiometric ages probably reflect diagenetic alteration, and a few of the pre-middle Miocene dates may prove to be useful in future recalibrations of the Cenozoic time scale. For purposes of this discussion we consider some of the incongruent results in the context of possible diagenetic influences. For example, there is a significant disparity between the $^{40}Ar/^{39}Ar$ ages and the biostratigraphic ages of two lower middle Miocene–upper lower Miocene tephras from Hole 999A (Samples 165-999A-41X-4, 41–42 cm, and 45X-2, 94–95 cm; 378.61 and 414.54 mbsf, respectively); yet the upper lower Miocene tephra in Sample 165-999A-48X-6, 42–43 cm (449.02 mbsf) yields an excellent age that is identical to the nannofossil age. However, we also note that although the biotite age of Sample 165-999A-48X-6, 42–43 cm, is congruent with the biostratigraphic age, the sanidine age is ~1.6 m.y. younger. Another example of within-site variability comes from the lower Miocene tephras in Hole 998A. The tephra layer in Sample 165-998A-27X-1, 120–122 cm (244.40 mbsf), yields an age that is in excellent agreement with the nannofossil age, whereas the tephra at 29X-3, 68–69 cm (266.18 mbsf), is ~3 m.y. older than the biostratigraphic age. A replicate analysis from the latter tephra gives an age that is 10 Ma younger. The lower Miocene at Site 1000 also shows significant disparities between the radiometric and biostratigraphic ages. In this case, the three lower Miocene tephras analyzed in this study yield ages that are inverted; the stratigraphically highest of the three (Sample 165-1000B-14R-2, 139–140 cm; 611.77 mbsf) yields the oldest radiometric age (18.31 Ma), whereas the stratigraphically lowest of these tephras (19R-2, 99–101 cm; 659.89 mbsf) yields the youngest radiometric age (17.02 Ma; Table 1).

In general, there is less agreement between the tephra ages and the biostratigraphic ages in the Oligocene part of the section. Two of the three Oligocene tephras analyzed in this study, one from Sample 165-

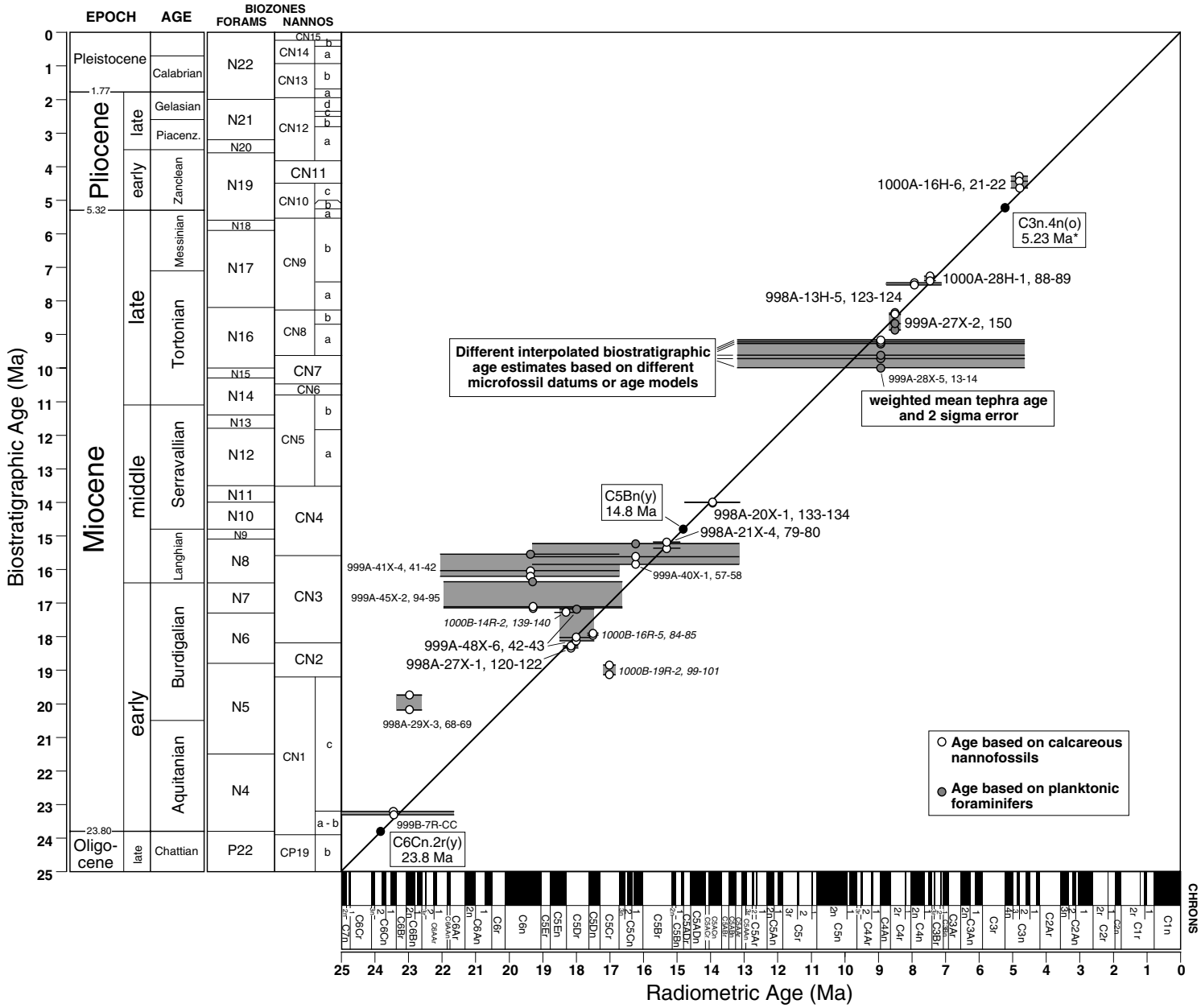

Figure 4. Comparison of radiometric dates of Caribbean tephra layers and the Neogene biostratigraphic ages correlated to the Berggren et al. (1995a) time scale. The black circles show calibration ages used in the Berggren et al. (1995b) age model. The $^{40}Ar/^{39}Ar$ ages are shown with 2-σ error bars. Data are presented in Table 2. Ma* = ages of magnetic reversals for Subchron C3n.4n(o) and younger have been calibrated to the astronomical time scale of Shackleton et al. (1990), Hilgen (1991), Langereis et al. (1994), and Berggren et al. (1995a).

999B-15R-2, 45–46 cm (661.05 mbsf) and the other from 1R-7, 53–54 cm (567.30 mbsf), produced radiometric ages that are close to the biostratigraphic ages, but the means suggest some differences. Provided these tephras have not been diagenetically altered, the results may indicate that either the nannofossil datums used for the Oligocene need further refinement or the polarity time scale needs additional age calibration points in the Oligocene. There is good congruence between radiometric and biostratigraphic ages in the lower Eocene of Site 999 (Sample 165-999B-48R-3, 6–7 cm), yet there is significant disparity between the two geochronologies in another lower Eocene sample from the same site (Sample 165-999B-47R-6, 4–5 cm). The three late Paleocene tephra layers from Site 1001 analyzed in this study are highly incongruent with the biostratigraphic ages. The most likely explanation is that these tephras have been diagenetically altered (see below).

Interstitial pore fluid movement through some of these coarse-grained tephra layers may be at least partially responsible for the incongruent results between radiometric ages and biostratigraphic ages. The distinctive diagenetic profiles of Sites 998–1001 illustrate the migration of chemical species through the sedimentary column (Sigurdsson, Leckie, Acton, et al., 1997; Lyons et al., Chap. 19, this volume). For example, microbially mediated redox diagenesis characterizes the lower and middle Miocene at Site 1000 (Lyons et al., Chap. 19, this volume). In addition, elevated levels of dissolved silica characterize the middle Miocene and older sections at Sites 998, 999, and 1001 indicating diagenetic changes and movement of pore fluids in the deeper parts of each section (Lyons et al., Chap. 19, this volume). Note for example that the radiometric ages are highly congruent with the biostratigraphic ages at Site 998 down to a level near the highest occurrence of diagenetic chert at ~248 mbsf. Mineral grains analyzed from three tephra layers at Site 1001 were most likely altered by diagenesis based on the highly incongruent results. Redeposition of volcanic debris is an unlikely explanation for the spurious ages because these particular layers resemble all the other numerous thick tephras cored during Leg 165. Although the tephra layers often do contain coarser mineral grains at the base thereby resembling a graded bed, the tephras do not show the distinctive scoured basal contact or the rippled to parallel laminations expected in the upper part of turbidite deposits. Fabricius (Chap. 10, this volume) concluded that ~400 m of section has been removed beneath the middle Miocene–Eocene unconformity at this site, based on a study of the physical properties and the presence of microstylolites in these deeply buried carbonate-rich rocks.

The Caribbean Oceanic Plateau

The most voluminous volcanism in the Caribbean region occurred in the submarine environment, producing an oceanic plateau. Most of the information on the oceanic plateau has come from studies at its exposed subaerial margins on the perimeter of the Caribbean plate (Duncan and Hargraves, 1984; Sinton et al., 1998). This oceanic plateau is up to 20 km thick, and at least 600,000 km^2 in lateral extent. During Leg 165, the oceanic crust of the plateau was sampled at Site 1001 on the lower Nicaraguan Rise, with a penetration of 38 m into a succession of submarine basalt lavas. Some of these basalts are exceptionally fresh, as evidenced by the preservation of basaltic glass. The $^{40}Ar/^{39}Ar$ dating of these basalts yielded an age of 81 ± 1 Ma, in agreement with earlier dating of the plateau (Sinton et al., Chap. 15, this volume). These dates are particularly important, in that the dated rocks are demonstrably submarine lavas that predate the overlying mid-Campanian calcareous sediment, and thus provide a reliable age of the beginning of burial of the oceanic plateau in this region (Sigurdsson, Leckie, Acton, et al., 1997). Benthic foraminiferal evidence suggests that the plateau subsided from upper bathyal depths (200–500 m) in early to mid-Campanian time to middle or lower bathyal depths (1000–2500 m) by the late Maastrichtian.

A number of volcaniclastic turbidites and volcanic ash layers are found in the Paleocene carbonate sediment 158–255 m above the submarine basalt formation at Site 1001, and biotites were extracted from three of these layers for $^{40}Ar/^{39}Ar$ dating (Table 2). However, the biotites yield apparent ages that are well in excess of the biostratigraphic age of the adjacent sediment. This discrepancy is attributed to cryptic alteration of the biotites, as they occur in ash layers where virtually all of the volcanic glass has been altered to smectite.

The Cayman Ridge

One of the earliest known episodes of explosive volcanism in the circum-Caribbean region is represented by a late Paleocene to middle Eocene island arc that extended from the submerged Cayman Ridge in the west to the now-exposed Sierra Maestra province of eastern Cuba (Draper and Barros, 1994; Iturralde-Vinent, 1996). Drilling at Site 998 on the north flank of the Cayman Rise during Leg 165 led to the discovery of a major lower to middle Eocene volcanic ash and volcaniclastic turbidite succession that we correlate with the Sierra Maestra arc of Cuba (Sigurdsson, Leckie, Acton, et al., 1997), although a source in the Newcastle and Summerfield formations of Jamaica cannot be ruled out. At this ODP site, the frequency and thickness of ash layers and turbidites increases progressively with depth through the middle to lower Eocene section, and drilling at this site was terminated before the volcaniclastic-rich sequence was fully penetrated. At Site 999, lower Eocene tephra fallout layers form a weak, but significant peak in ash accumulation rate in the 50-Ma range, and biotites from two of these layers were selected for $^{40}Ar/^{39}Ar$ dating (Tables 1, 2). They yield ages of 48.6 and 52.5 Ma. Tephra layers and volcaniclastic turbidites in this episode at Site 998 did not contain biotites suitable for dating.

Seismic data suggest that basement rocks at Site 998 are ~210 m below the bottom of the hole, indicating that this part of the Cayman Rise is a volcanic arc, most likely continuous with the Paleocene–Eocene Sierra Maestra arc. Studies of the Sierra Maestra terrain provide clues about the arc structure underlying Site 998, some 750 km to the west. The volcanic Turquino zone is a major part of the Sierra Maestra region in southeast Cuba, and it is flanked to the north by the sedimentary and volcaniclastic Cauto zone, which has been interpreted as a backarc basin (Cobiella-Reguera, 1988, 1997). The Turquino succession, which rests on Cretaceous volcaniclastics, is composed of calc-alkaline basaltic to rhyolitic lavas and pyroclastics, with thin intercalations of marine sediments ranging from Danian to Eocene in age. The volcanic succession, which is several kilometers in thickness, is intruded locally by younger granites that range in age from 46 to 58 Ma (Khudoley and Meyerhoff, 1971).

An integrated picture of evidence from drilling at Site 998, from the Sierra Maestra in Cuba and from dredging of the north wall of the Cayman Trough (Perfit and Heezen, 1978), is of an east-west–trending island arc in Paleocene-Eocene time, shedding off volcaniclastic turbidites and tephra fallout into the Yucatan Basin to the north (Fig. 5). The polarity of subduction beneath the arc has a fundamental bearing on tectonics in the Caribbean region. We have previously proposed that subduction of the leading edge of the Caribbean plate beneath the Cayman Rise was from the south (Sigurdsson, Leckie, Acton, et al., 1997), which is in agreement with tectonic models proposed for the Sierra Maestra segment of the arc in Cuba (Iturralde-Vinent, 1996; Cobiella-Reguera, 1997). The principal implications of this conclusion are, first, that the Caribbean plate had a strong vector of northward motion in the Paleogene and, second, that the leading edge of the plate was subducted and thus relatively thin oceanic crust, as opposed to the thick oceanic plateau that makes up much of the plate interior. It is likely, as inferred in Figure 5, that the Aves Ridge was the eastern and southern continuation of the Cayman Ridge, as radiometric dates of granodiorites dredged from the Aves Ridge yield Late Cretaceous to early Tertiary ages (Fox et al., 1971). We note that

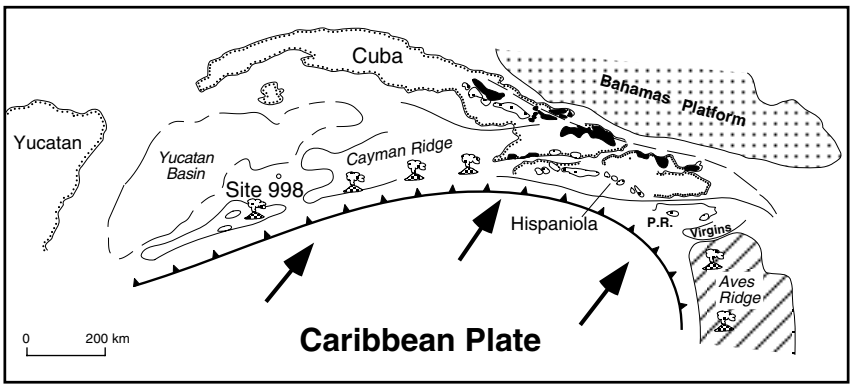

Figure 5. The plate tectonic configuration of the volcanic arc that comprised the Cayman Rise and the Sierra Maestra volcanic terrain of Cuba during early Eocene time, based on results from drilling at Site 998 (Sigurdsson, Leckie, Acton, et al. 1997). To the east, the Cayman arc may have had its continuation in the Aves arc, active in Late Cretaceous to early Tertiary (Fox et al., 1971).

a southwest-dipping seismic zone has also been proposed for the Cayman Rise (Pindell and Barrett 1990; Pindell 1994; Draper et al., 1994), and thus, the plate tectonic configuration of this area still remains unresolved.

The geographic extent of tephra fallout from explosive volcanism of the Cayman Ridge and Sierra Maestra volcanic arc also includes the region of the Nicaraguan Rise, as indicated by recovery of large numbers of tephra layers in upper Paleocene and lower Eocene sediments at Site 1001. At the time of this activity, Site 1001 was probably due south of the Cayman Ridge, if we backtrack the transcurrent motion on the Cayman trench fracture zone since the Eocene. At this time, Jamaica would have been in an intermediate position with respect to the Nicaraguan Rise and the Cayman Ridge, or perhaps somewhat further to the west. Contemporaneous volcaniclastics interbedded with sediments are found in the Summerfield Formation and the Wagwater Formation in Jamaica (Robinson, 1994), and may correlate with the Paleocene–Eocene episode of explosive volcanism documented during Leg 165. In Hispaniola, lower Tertiary formations provide evidence of volcanic arc construction in the Paleocene to Eocene (Draper et al., 1994).

Eocene Explosive Volcanism

The largest episode of explosive volcanism documented in Leg 165 sediments began in the middle Eocene (~46 Ma) and terminated in the early Oligocene (~32 Ma). This episode is particularly well recorded at Site 999 on the Kogi Rise, Colombian Basin, but is also present in sediments at Site 998 on the Cayman Rise. At Site 999, the accumulation rate of tephra is ~250 cm/m.y., and the frequency of major explosive eruptions in the source region(s) is on the order of one event per 20 k.y. The rhyolitic tephra layers are generally 2–5 cm in thickness. Biotites from two tephra layers at Site 998, representing the late stages of this episode, were dated by the $^{40}Ar/^{39}Ar$ technique, yielding ages of 30.7 and 31.7 Ma (Tables 1, 2). Tephra layers at Site 999 from this episode do not contain biotites suitable for dating. Considering that Site 999 is over 600 km from a possible volcanic source, it is evident that these fallout deposits represent major ignimbrite-forming events. The thickness-distance relationship of the tephra layers suggests a magnitude (volume) for these eruptions in the range of the 30-k.y. eruption from the Phlegrean Fields caldera in Italy (100 km^3) and the 75-k.y. Toba eruption on Sumatra (2000 km^3).

The source of these tephra layers is most likely to be found in Central America. Two major Tertiary ignimbrite formations extend from the Mexican border in the north, through Guatemala, El Salvador and Honduras, into Nicaragua, over a region that is more than 800 km in length and up to 300 km wide. They represent the largest episode of silicic ignimbrite volcanism in Central America. The ignimbrite-rich formations underlie upper Tertiary and Quaternary andesitic and basaltic andesite stratocones of the active Central American volcanic arc (Reynolds, 1980). However, the Tertiary ignimbrite-bearing formations generally extend far east of the active arc. We have earlier proposed that the Eocene tephra fallout episode found during Leg 165 correlates with the ignimbrite-producing events represented by the Matagalpa and Morazan Formations of Central America (Sigurdsson, Leckie, Acton, et al., 1997). The latter formations were tentatively given an early Oligocene age by Ehrenborg (1996) on the basis of meager radiometric data, but the deep-sea evidence from Leg 165, including data presented here, indicates that these ignimbrites were dominantly erupted during the Eocene. A pre-Miocene ignimbrite series has been recognized in Central America for some time, and it is now becoming accepted as a widespread lithostratigraphic unit. In both Guatemala and El Salvador, older Tertiary (pre-Miocene) rhyolitic tuffs are present, but generally unnamed and unmapped, or grouped in the Morazan Formation (El Salvador). In the Nicaraguan Highlands, the Matagalpa Group is unconformably overlain by the Miocene Coyol Group. The Matagalpa Group is dominated by 50-m-thick dacite to rhyolite ignimbrites and associated tephra fall deposits, with a total thickness in excess of 2 km (Ehrenborg, 1996).

The Central American Eocene–early Oligocene volcanic episode recorded in Leg 165 sediments is broadly contemporaneous with the rhyolitic ignimbrite flare-up in the Sierra Madre Occidental province of Mexico (Fig. 8). The Sierra Madre Occidental is Earth's largest ignimbrite province, with an areal extent of ~250,000 km^2 and over 1 km in thickness (McDowell and Clabaugh, 1979). The initiation of these contemporaneous episodes of siliceous volcanism in Central America and Mexico may be related to plate tectonic rearrangements in the Pacific Ocean. They coincide broadly with the abrupt change in the direction of motion of the Pacific plate at 43 Ma, from northwesterly to a more westerly direction, as recorded by the bend (60°) in the Emperor-Hawaiian hot spot chain (Atwater, 1970, 1989).

Miocene Explosive Volcanism

Sites 998, 999, and 1000 recovered a large number of tephra fall layers that constitute a major episode of Miocene silicic explosive volcanism in the Caribbean region, comparable in magnitude and character to the Eocene event, although individual tephra layers tend to be thicker in the Miocene episode (Fig. 6). At all three sites, the siliceous tephra layers have the characteristics of co-ignimbrite fallout deposits (Sigurdsson, Leckie, Acton, et al., 1997; Carey and Sigurdsson, Chap. 5, this volume). The distribution and thickness of the Miocene tephra at these three sites indicates a general fallout axis trending easterly out of Central America, the nearest major source of ignimbrite volcanism in the late Tertiary (Fig. 7).

As shown in Figure 2, the Miocene tephra accumulation at Site 999 defines a rather sharp peak at ~19 Ma, beginning near the Oligocene/Miocene boundary (~23 Ma) and terminating in the middle Miocene at ~13 Ma. Biotites from 18 Miocene tephra layers from all three sites were dated by the $^{40}Ar/^{39}Ar$ technique (Tables 1, 2) and

sanidine crystals were $^{40}Ar/^{39}Ar$ dated in one layer (Table 3). Ages of most of the dated layers fall within the range of the peak in accumulation rate, as this part of the record contains the most abundant and thickest layers suitable for crystal extraction. As shown in Figure 2, a subsidiary peak in ash accumulation occurs in the range of 8–10 Ma.

The Miocene tephra episode recorded in the Caribbean sediments is likely to represent the distal fallout equivalent of thick ignimbrite formations that are present throughout Central America. The major formations include silicic welded tuffs of the Chalatenango Formation in south-central Guatemala and El Salvador (Reynolds, 1987; Wiesemann, 1975), thick rhyolitic ignimbrites of the Padre Miguel Group in southeast Guatemala and Honduras (Reynolds, 1980), and the thick siliceous ignimbrites of the Coyol Group in Nicaragua (Ehrenborg, 1996). Reliable $^{40}Ar/^{39}Ar$ single crystal biotite ages for ignimbrites within the Coyol Group cluster from 12.3 to 18.4 Ma, defining an early–middle Miocene volcanic episode. Many of the formations are linked to caldera structures and have aggregate thicknesses of several hundred meters. Some of the co-ignimbrite tephra from eruptions of this ignimbrite province were transported into the Pacific, where it was recovered off Guatemala during Deep Sea Drilling Program (DSDP) Leg 67 (Cadet et al., 1982a), and near the Middle America Trench off Mexico during Leg 66 (Cadet et al., 1982b). However, as we would predict from atmospheric circulation (Carey and Sigurdsson, Chap. 5, this volume, the dispersal and accumulation rate to the west is minor, compared to the easterly fallout pattern in the Caribbean.

A relationship between a change in the plate tectonic configuration and origin of the Central American ignimbrite episodes is as yet unclear, but some factors suggest a connection. The onset of the Miocene episode at ~23 Ma coincides with a major tectonic reconfiguration in the eastern Pacific, adjacent to the Central American arc. Magnetic anomalies on the Pacific and Nazca (Farallon) plates show an abrupt change in trend between anomalies generated during the Miocene and the Oligocene, requiring a major reorientation of spreading dynamics (Handschumacher, 1976). Subduction of the Farallon plate during the Oligocene was nearly due east below Central America, at a rate of 6.5 cm/yr. Because of the subduction of the Farallon-Pacific spreading ridge below North America, a direct coupling of the American-Pacific plate occurred at ~26 Ma, resulting in a radical change in spreading kinematics in the eastern Pacific. This brought about north-south spreading from a new east-west–trending Cocos-Nazca spreading center, beginning between 20 and 25 Ma, dividing the Farallon plate into the Nazca and Cocos plates (Handschumacher, 1976; Duncan and Hargraves, 1984; Meschede et al. 1998). This led to a change in subduction of the Cocos plate beneath Central America, to a more northeasterly direction, at a higher rate of ~7 cm/yr. We speculate that this is what initiated the onset of the large Miocene ignimbrite flare-up on the Chortis block in Central America.

DISCUSSION AND CONCLUSIONS

A principal discovery from Leg 165 drilling in the western Caribbean was the identification of three major episodes of explosive volcanism that occurred during the last 55 m.y. on the margins of the evolving Caribbean Basin. These episodes can be clearly related to regional sources, but how do these events compare with the global record of explosive volcanism? Kennett and Thunnell (1975) first pointed out that the frequency of volcanic ash layers in deep-sea sediments is episodic with pronounced peaks in the Quaternary (last 2 m.y.) and the middle Miocene (14–16 Ma). They suggested that these episodes were global in nature and related to large-scale plate tectonic processes. Subsequent studies have also shown evidence for broad global synchronism in volcanic ash deposition in the ocean basins (Kennett and Thunnell, 1977; Kennett, 1981). These observations were further supported by later results from DSDP sites with better

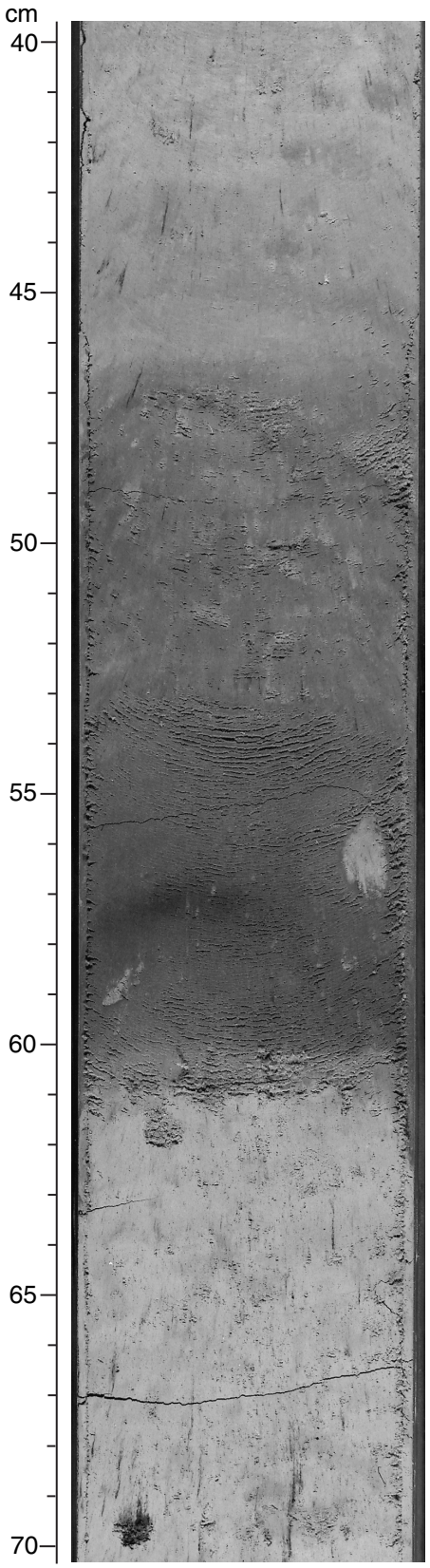

Figure 6. Photograph of a typical Miocene silicic tephra fall layer in a Leg 165 sediment core, showing a sharp base and a gradational bioturbated top (Sample 165-1000A-22H-2, 40–70 cm).

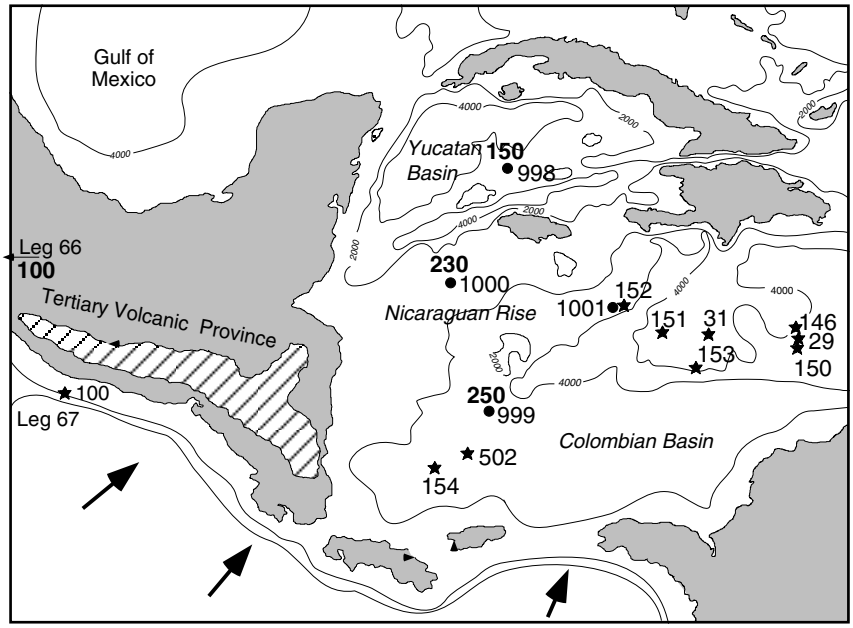

Figure 7. The relationship between Miocene Central American ignimbrite volcanism (Tertiary volcanic province) and the Miocene tephra fallout record observed in Caribbean sediments drilled during Leg 165. Numbers at solid circles indicate site locations; boldface numbers refer to the Miocene peak ash layer accumulation rate (in centimeters per million years). Stars indicate location of DSDP sites. The map represents a paleogeographic reconstruction based on inferred transcurrent motion of the Cayman Trench since the Miocene (Sigurdsson, Leckie, Acton, et al., 1997).

core recovery (Cadet and Fujioka, 1980; Cadet et al., 1982a, 1982b; Cambray and Cadet, 1996). Compared to these studies, however, the Caribbean sites are characterized by a conspicuous lack of a late Quaternary peak and an offset between the global mid-Miocene peak and the early- to mid-Miocene peak seen at Sites 998, 999, and 1000.

Comparison with tephra layer distributions in a number of other ODP and DSDP sites (Cambray and Cadet, 1996) indicates that explosive volcanic activity also increased globally during the Eocene, and thus the Caribbean Eocene volcanic episode also has contemporaneous equivalents in many other arcs. Data on the global volcanic ash distribution during the Paleogene are much poorer at sites outside the Caribbean, however, as many drill sites do not penetrate to this depth.

Thus the Caribbean episodes discussed above, and evidence from earlier compilations of tephra episodes from ODP and DSDP sites in other ocean basins, indicate two major global pulses of explosive volcanic activity. We note, however, that the drilled marine record does not as yet include adequate sampling of volcanic ash falls from the greatest ignimbrite flare up on Earth: the Sierra Madre Occidental in Mexico. On the basis of normal atmospheric transport and fallout patterns, it is likely that tephra layer deposits from this volcanic episode are to be found in the Gulf of Mexico, a region that has not experienced scientific drilling since DSDP Leg 10 (Worzel et al., 1973). Because of very poor core recovery, information on tephra distribution from Leg 10 drilling in the Gulf of Mexico is scanty, but lower Oligocene tephra layers were observed at DSDP Site 94, and Sites 86, 94, 95, 96, and 97 also contain common ash layers (Worzel et al., 1973). The Sierra Madre Occidental activity is quite extensive in space and time, ranging from 47 to 27 Ma (McDowell and Mauger, 1994), and its northward continuation, the San Juan and the Mogollon-Datil volcanic fields, extend the record of large-scale explosive volcanism in this region up to 25 Ma, or spanning all of the Oligocene. When taken together, the combined land and marine evidence shows that the Paleogene ignimbrite activity of the Central American and Mexican arcs thus spans the mid- to late Eocene and most of the Oligocene (Fig. 8).

As shown by a comparison of the major volcanic episodes with the oxygen isotope evidence in Figure 8, major oxygen isotope enrichments in benthic $\delta^{18}O$ exhibit some coincidence with these volcanic episodes, suggesting that some connection may exist between the intensified volcanic activity and climate change in the Cenozoic, particularly during the late Eocene and Oligocene.

The concept of global synchroneity of explosive volcanism is difficult to reconcile with the paradigm of plate tectonics. At any one time, the various subduction zones on Earth experience a spectrum of the parameters that may affect the rates of subduction zone volcanism, such as the rates and direction of plate motion, and age and composition of the subducting slab. No unifying mechanism is obvious that could lead to a simultaneous increase in global eruption rates. A possible exception to this may be the rate of sediment subduction. The high global rate of explosive volcanism in the Quaternary could possibly be related to increased availability of sediment for subduction (von Huene and Scholl, 1991). Such a hypothesis does not account, however, for the Miocene and Eocene explosive volcanic episodes documented here.

It has been proposed (Sigurdsson, 1990a) that the global episodic ash layer frequency in deep-sea sediments may be influenced by a transport function, such as major climate-related variations in the global atmospheric circulation and tephra dispersal. Evidence from marine sediments supports the idea that the observed variations in deposition rate of some deep-sea volcanic ash layers may be influenced by transport processes (i.e., the vigor of atmospheric circulation). For example, data from DSDP Site 284 show peaks in ash abundance coinciding with glacial episodes during the latest Miocene, late Pliocene and the Quaternary (Shackleton and Kennett, 1975; Kennett et al., 1979). Similarly, early studies showed that the peak periods of eolian transport and strong atmospheric circulation coincide with the episodes of volcanic ash deposition (Leinen and Heath, 1981; Leinen, 1985; Rea et al., 1985). This coincidence may indicate that volcanic ash frequency may not simply be an indicator of variations in the volcanic source function, but may also be influenced by the rate of transport (i.e., climate-related variations in the vigor of atmospheric circulation). Conversely, the relationship between the intensity of volcanism and climate may result from crustal dynamics affected by changes in sea level and glacier loading. However, in reviewing the marine eolian deposition on the basis of evidence from a sediment core from the central gyre of the North Pacific, Rea (1994) concludes that dust size increases progressively from 50 Ma to present, with some oscillations, but no distinct peaks during the mid-Miocene or Quaternary. Similarly, the dust flux in this core shows a dramatic increase at 3 Ma (onset of Northern Hemisphere glaciation), but this is primarily an aridity change, not a wind intensity shift.

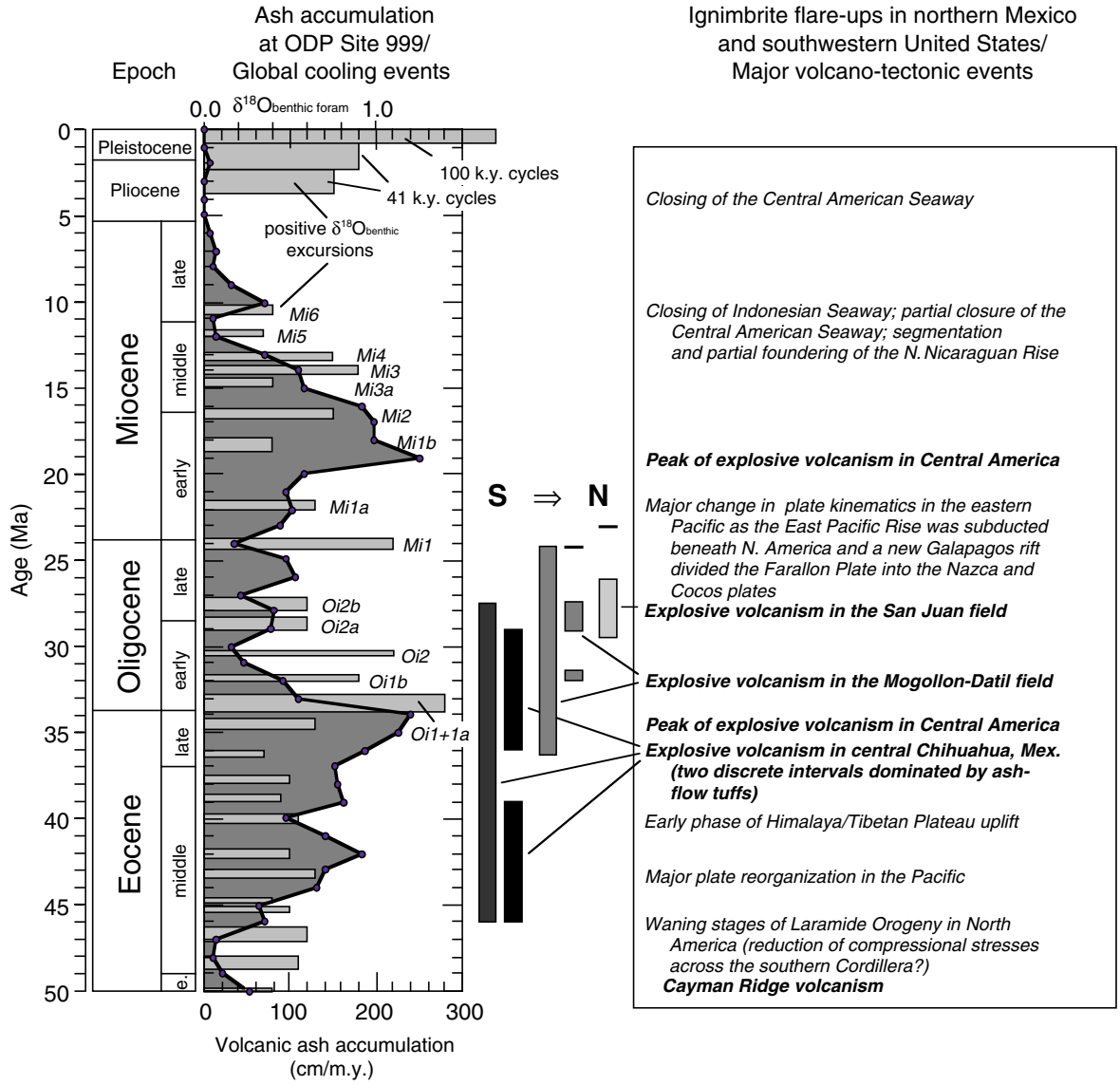

Figure 8. A comparison of the Caribbean record of explosive volcanism (tephra accumulation rate at ODP Site 999), compared with global cooling events (positive $\delta^{18}O$ excursions) through the last 50 m.y. of the Cenozoic. Also shown are periods of major ignimbrite volcanism in northern Mexico and the southwestern United States (McDowell and Mauger, 1994). Isotopic data from multiple sources: Mix et al. (1995; Pliocene–Pleistocene), Miller et al. (1996, 1998; Miocene), Pekar and Miller (1996; Oligocene), and Zachos (in Baker and McNutt, 1998; Eocene). Labeled oxygen isotope events of the Oligocene and Miocene are after Miller et al. (1996).

Thus the causes of the global episodes in deep-sea tephra deposition remain poorly understood, and the relative importance of the variable intensity of both source and transport mechanisms needs to be unraveled. On land, however, we have clear indication that volcanism in the source regions is highly episodic, and a tectonic forcing function is a most likely explanation.

Do these silicic magmas represent true addition of new continental crust, or are they largely recycled or reworked continental material, with minor addition of mantle-derived material? Two contrasting models have been proposed: (1) crustal melting by influx of basaltic magma from the mantle (Verma, 1984; Ruiz et al., 1988); and (2) fractional crystallization from primary basaltic magma (Cameron et al., 1980; Smith et al., 1996). Intermediate models propose crustal magmatism as a result of assimilation fractional crystallization (AFC) between basaltic magma and the crust (Smith et al., 1996). In the case of crustal melting, the basalt volume may be approximately equal to the amount of melted crust. In the case of fractional crystallization, the fraction of basaltic melt would be considerably higher than the derived silicic magma. A central implication of these models is that a large volume of basaltic magma was available, either supplying heat for crustal melting (Reiners et al., 1995), or as primary magma for fractionation to generate voluminous silicic differentiates. The requirements for basaltic magma are truly large. In the Sierra Madre Occidental volcanic arc, for example, the volcanic extrusion rate of silicic magmas was probably of the order 20 km^3/m.y./km arc during the Eocene–Oligocene episode. By comparison, the modern volcanic flux of the Central American arc is only 0.1–1 km^3/m.y./km (Carr et al., 1990). This silicic magma flux would require a supply rate of basaltic magma of the order of 100 km^3/m.y./km for fractionation and AFC scenarios, and no less than 50 km^3/m.y./km for dominantly crustal melting scenarios, as compared to 1–9 km^3/m.y./km magma extrusion rates in modern arcs (Sugimura et al., 1963; McBirney,

1978; Sigurdsson et al., 1980; Bloomer et al., 1989; Sigurdsson, 1990b).

REFERENCES

Adams, C.J., and Kelley, S.P., 1997. Provenance of Permo-Triassic and Ordovician Metagreywake Terranes in New Zealand: evidence from $^{40}Ar/^{39}Ar$ dating of detrital micas. *Geol. Soc. Am. Bull.,* 110:422–432.

Atwater, T., 1970. Implications of plate tectonics for the Cenozoic tectonic evolution of western North America. *Geol. Soc. Am. Bull.,* 81:3513–3536.

————, 1989. Plate tectonic history of the northeast Pacific and western North America. *In* Winterer, E.L., Hussong, D.M., and Decker, R.W. (Eds.), *The Eastern Pacific Ocean and Hawaii.* Geol. Soc. Am., Geol. of North America Ser., N:21–72.

Backman, J., and Raffi, I., 1997. Calibration of Miocene nannofossil events to orbitally tuned cyclostratigraphies from Ceara Rise. *In* Shackleton, N.J., Curry, W.B., Richter, C., and Bralower, T.J. (Eds.), *Proc. ODP, Sci. Results,* 154: College Station, TX (Ocean Drilling Program), 83–99.

Baker, P., and McNutt, M. (Eds.), 1998. *The Future of Marine Geology and Geophysics (FUMAGES).* Proc. Workshop, Washington, Nat. Sci. Found., December, 1996.

Berggren, W.A., Hilgen, F.J., Langereis, C.G., Kent, D.V., Obradovich, J.D., Raffi, I., Raymo, M.E., and Shackleton, N.J., 1995a. Late Neogene chronology: new perspectives in high-resolution stratigraphy. *Geol. Soc. Am. Bull.,* 107:1272–1287.

Berggren, W.A., Kent, D.V., Swisher, C.C., III, and Aubry, M.-P., 1995b. A revised Cenozoic geochronology and chronostratigraphy. *In* Berggren, W.A., Kent, D.V., Aubry, M.-P., and Hardenbol, J. (Eds.), *Geochronology, Time Scales and Global Stratigraphic Correlation.* Spec. Publ.—Soc. Econ. Paleontol. Mineral. (Soc. Sediment. Geol.), 54:129–212.

Bloomer, S.H., Stern, R.J., and Smoot, N.C., 1989. Physical volcanology of the submarine Mariana and Volcano arcs. *Bull. Volcanol.,* 51:210–224.

Cadet, J.-P., and Fujioka, K., 1980. Neogene volcanic ashes and explosive volcanism: Japan Trench transect, Leg 57, Deep Sea Drilling Project. *In* von Huene, R., Nasu, N., et al., *Init. Repts. DSDP,* 56, 57 (Pt. 2): Washington (U.S. Govt. Printing Office), 1027–1041.

Cadet, J.-P., Pouclet, A., Thisse, Y., Bardintzeff, J.M., and Azéma, J., 1982a. Middle America Neogene explosive volcanism and ash layers: evidence from the Middle America trench transect, Deep Sea Drilling Project Leg 67. *In* Aubouin, J., von Huene, R., et al., *Init. Repts. DSDP,* 67: Washington (U.S. Govt. Printing Office), 475–491.

Cadet, J.-P., Thisse, Y., Pouclet, A., Bardintzeff, J.M., and Stephan, J.F., 1982b. Tephra from Deep Sea Drilling Project Leg 66: Middle American Trench Transect (Southern Mexico). *In* Watkins, J.S., Moore, J.C., et al., *Init. Repts. DSDP,* 66: Washington (U.S. Govt. Printing Office), 687–698.

Cambray, H., and Cadet, J.P., 1996. Synchronisme de l'activite volcanique d'arc: mythe ou realite? *C.R. Acad. Sci. Ser. 2,* 322:237–244.

Cameron, M., Bagby, W.C., and Cameron, K.L., 1980. Petrogenesis of voluminous mid-Tertiary ignimbrites of the Sierra Madre Occidental, Chiuahua, Mexico. *Contrib. Mineral. Petrol.,* 74:271–284.

Cande, S.C., and Kent, D.V., 1992. A new geomagnetic polarity time scale for the Late Cretaceous and Cenozoic. *J. Geophys. Res.,* 97:13917–13951.

————, 1995. Revised calibration of the geomagnetic polarity timescale for the Late Cretaceous and Cenozoic. *J. Geophys. Res.,* 100:6093–6095.

Carr, M.J., Feigenson, M.D., and Bennett, E.A., 1990. Incompatible element and isotopic evidence for tectonic control of source mixing and melt extraction along the Central American arc. *Contrib. Mineral. Petrol.,* 105:369–380.

Chaisson, W.P., and Pearson, P.N., 1997. Planktonic foraminifer biostratigraphy at Site 925: middle Miocene–Pleistocene. *In* Shackleton, N.J., Curry, W.B., Richter, C., and Bralower, T.J. (Eds.), *Proc. ODP, Sci. Results,* 154: College Station, TX (Ocean Drilling Program), 3–31.

Chesner, C.A., Rose, W.I., Deino, A., Drake, R., and Westgate, J.A., 1991. Eruptive history of Earth's largest Quaternary caldera (Toba, Indonesia) clarified. *Geology,* 19:200–203.

Cobiella-Reguera, J.L., 1988. El volcanismo paleogenico cubano: apuntes para un nuevo enfoque. *Rev. Tecnol.,* 18:25–32.

————, 1997. Zonacion estructuro facial del corte Paleoceno Eoceno medio de Cuba. *Rev. Miner. Geol.,* 14:3–12.

Crowley, T.J., Christie, T.A., and Smith, N.R., 1993. Reassessment of Crete (Greenland) ice core acidity/volcanism link to climate change. *Geophys. Res. Lett.,* 20:209–212.

Draper, G., and Barros, J.A., 1994. Cuba. *In* Donovan, S.K., and Jackson, T.A. (Eds.), *Caribbean Geology: an Introduction:* Jamaica (Univ. of the West Indies Publ.), 65–86.

Draper, G., Mann, P., and Lewis, J.F., 1994. Hispaniola. *In* Donovan, S.K., and Jackson, T.A. (Eds.), *Caribbean Geology: an Introduction:* Jamaica (Univ. of the West Indies Publ.), 129–150.

Duncan, W.M., and Hargraves, R.B., 1984. Plate tectonic evolution of the Caribbean region in the mantle reference frame. *I*n Bonini, W.E., Hargraves, R.B., and Shagam, R. (Eds.), *The Caribbean-South American Plate Boundary and Regional Tectonics.* Mem.—Geol. Soc. Am., 162:81–83.

Ehrenborg, J., 1996. A new stratigraphy for the Tertiary volcanic rocks of the Nicaraguan Highland. *Geol. Soc. Am. Bull.,* 108:830–842.

Fox, P.J., Schreiber, E., and Heezen, B.C., 1971. The geology of the Caribbean crust: Tertiary sediments, granitic and basic rocks from the Aves Ridge. *Tectonophysics,* 12:89–109.

Handschumacher, D.W., 1976. Post-Eocene plate tectonics of the Eastern Pacific. *In* Sutton, G.M., et al. (Eds.), The Geophysics of the Pacific Ocean Basin and its Margin. *Am. Geophys. Union Monogr.,* 19:177–202.

Hilgen, F.J., 1991. Extension of the astronomically calibrated (polarity) time scale to the Miocene/Pliocene boundary. *Earth Planet. Sci. Lett.,* 107:349–368.

Iturralde-Vinent, M.A., 1996. Cuba: El archipelago volcanico Paleoceno-Eoceno medio. *In* Iturralde-Vinent, M.A. (Ed.), *Ofiolitas y Arcos Volcanicos de Cuba. Project 364, Caribbean Ophiolites and Volcanic Arcs.* IGCP-UNESCO, 231–246.

Kelley, S.P., 1995. The laser microprobe Ar-Ar technique of dating. *In* Potts, P.J., Bowles, J.F.W., Reed, S.J.B., and Cave, M.R. (Eds.), *Microprobe Techniques in the Earth Sciences:* Cambridge (Mcgraw Hill).

Kennett, J.P., 1981. Marine tephrochronology. *In* Emiliani, C. (Ed.), *The Sea* (Vol. 7): *The Oceanic Lithosphere:* New York (Wiley), 1373–1436.

Kennett, J.P., Shackleton, N.J., Margolis, S.V., Goodney, D.E., Dudley, W.C., Kroopnick, P.M., 1979. Late Cenozoic oxygen and carbon isotopic history and volcanic ash stratigraphy: DSDP Site 284, South Pacific. *Am. J. Sci.,* 279:52–69.

Kennett, J.P., and Thunnell, R.C., 1975. Global increase in Quaternary explosive volcanism. *Science,* 187:497–503.

————, 1977. On explosive Cenozoic volcanism and climatic implications. *Science,* 196:1231–1234.

Khudoley, K.M., and Meyerhoff, A.A., 1971. *Paleogeography and Geological History of the Greater Antilles.* Mem.—Conf. Geol. Caribe, 5:249.

Langereis, C.G., Van Hoof, A.M., and Hilgen, F.J., 1994. Steadying the rates. *Nature,* 369:615.

Leinen, M., 1985. Quartz content of Northwest Pacific Hole 576A and implications for Cenozoic eolian transport. *In* Heath, G.R., Burckle, L.H., et al., *Init. Repts. DSDP,* 86: Washington (U.S. Govt. Printing Office), 581–588.

Leinen, M., and Heath, G.R., 1981. Sedimentary indicators of atmospheric circulation in the Northern Hemisphere during the Cenozoic. *Palaeogeogr., Palaeoclimatol., Palaeoecol.,* 36:1–21.

Ludwig, K.R., 1998. *Using Isoplot/Ex Version 1.00: A Geochronological Toolkit for Microsoft Excel.* Berkeley Geochronol. Cent. Spec. Publ., No. 1:43.

McBirney, A.R., 1978. Volcanic evolution of the Cascade Range. *Annu. Rev. Earth Planet. Sci.,* 6:437–456.

McDougall, I., and Roksandic, Z., 1974. Total fusion $^{40}Ar/^{39}Ar$ ages using HIFAR reactor. *Geol. Soc. Aust. J.,* 21:81–89.

McDowell, F.W., and Clabaugh, S.E., 1979. Ignimbrites of the Sierra Madre Occidental and their relation to the tectonic history of western Mexico. *Spec. Pap.—Geol. Soc. Am.,* 180:113–124.

McDowell, F.W., and Mauger, R.L., 1994. K-Ar and U-Pb zircon chronology of Late Cretaceous and Tertiary magmatism in central Chiuahua State, Mexico. *Geol. Soc. Am. Bull.,* 106:118–132.

Meschede, M., Barckhausen, U., and Worm, H.-U., 1998. Extinct spreading on the Cocos Ridge. *Terra Nova,* 10:211–216.

Miller, K.G., Mountain, G.S., Browning, J.V., Kominz, M., Sugarman, P.J., Christie-Blick, N., Katz, M., and Wright, J.D., 1998. Cenozoic global sealevel, sequences, and the New Jersey transect: results from coastal plain and continental slope drilling. *Rev. Geophys.,* 36:569–601.

Miller, K.G., Mountain, G.S., the Leg 150 Shipboard Party and Members of the New Jersey Coastal Plain Drilling Project, 1996. Drilling and dating

New Jersey Oligocene-Miocene sequences: ice volume, global sea level and Exxon records. *Science,* 271:1092–1995.

Mix, A.C., Pisias, N.G., Rugh, W., Wilson, J., Morey, A., and Hagelberg, T.K., 1995. Benthic foraminifer stable isotope record from Site 849 (0–5 Ma): local and global climate changes. *In* Pisias, N.G., Mayer, L.A., Janecek, T.R., Palmer-Julson, A., and van Andel, T.H. (Eds.), *Proc. ODP, Sci. Results,* 138: College Station, TX (Ocean Drilling Program), 371–412.

Pearson, P.N., and Chaisson, W.P., 1997. Late Paleocene to middle Miocene planktonic foraminifer biostratigraphy of the Ceara Rise. *In* Shackleton, N.J., Curry, W.B., Richter, C., and Bralower, T.J. (Eds.), *Proc. ODP, Sci. Results,* 154: College Station, TX (Ocean Drilling Program), 33–68.

Pekar, S.F., and Miller, K.G., 1996. New Jersey Oligocene "Icehouse" sequences (ODP Leg 150X) correlated with global $\delta^{18}O$ and Exxon eustatic records. *Geology,* 24:567–570.

Perfit, M.R., and Heezen, B.C., 1978. The geology and evolution of the Cayman Trench. *Geol. Soc. Amer. Bull.,* 89:1155–1174.

Pindell, J.L., 1994. Evolution of the Gulf of Mexico and Caribbean. *In* Donovan, S., and Jackson, T.A. (Eds.), *Caribbean Geology: An Introduction:* Jamaica (Univ. of the West Indies Publ. Assoc.), 269–291.

Pindell, J.L., and Barrett, S.F., 1990. Geologic evolution of the Caribbean region: a plate-tectonic perspective. *In* Dengo, G., and Case, J.E. (Eds.), *The Caribbean Region.* Geol. Soc. Am., Geol. North. Am. Ser., H:405–432.

Raffi, I., and Flores, J.-A., 1995. Pleistocene through Miocene calcareous nannofossils from eastern equatorial Pacific Ocean. *In* Pisias, N.G., Mayer, L.A., Janecek, T.R., Palmer-Julson, A., and van Andel, T.H. (Eds.), *Proc. ODP, Sci. Results,* 138: College Station, TX (Ocean Drilling Program), 233–286.

Rea, D.K., 1994. The paleoclimatic record provided by eolian deposition in the deep sea: the geologic history of wind. *Rev. Geophys.,* 32:159–195.

Rea, D.K., Leinen, M., and Janecek, T.R., 1985. Geologic approach to the long-term history of atmospheric circulation. *Science,* 227:721–725.

Reiners, P.W., Nelson, B.K., and Ghiorso, M.S., 1995. Assimilation of felsic crust by basaltic magma: thermal limits and extents of crustal contamination of mantle-derived melts. *Geology,* 23:563–566.

Reynolds, J.H., 1980. Late Tertiary volcanic stratigraphy of northern Central America. *Bull. Volcanol.,* 43:601–607.

————, 1987. Timing and sources of Neogene and Quaternary volcanism in south-central Guatemala. *J. Volcanol. Geotherm. Res.,* 33:9–22.

Robinson, E., 1994. Jamaica. *In* Donovan, S.K., and Jackson, T.A. (Eds.), *Caribbean Geology: an Introduction:* Jamaica (Univ. of West Indies Publ.), 111–127.

Ruiz, J., Patchett, P.J., and Arculus, R.J., 1988. Nd-Sr isotope composition of lower crustal xenoliths - Evidence for the origin of mid-Tertiary felsic volcanics in Mexico. *Contrib. Mineral. Petrol.,* 99:36–43.

Shackleton, N.J., Baldauf, J.G., Flores, J.-A., Iwai, M., Moore, T.C., Jr., Raffi, I., and Vincent, E., 1995a. Biostratigraphic summary for Leg 138. *In* Pisias, N.G., Mayer, L.A., Janecek, T.R., Palmer-Julson, A., and van Andel, T.H. (Eds.), *Proc. ODP, Sci. Results,* 138: College Station, TX (Ocean Drilling Program), 517–536.

Shackleton, N.J., Berger, A., and Peltier, W.A., 1990. An alternative astronomical calibration of the lower Pleistocene timescale based on ODP Site 677. *Trans. R. Soc. Edinburgh: Earth Sci.,* 81:251–261.

Shackleton, N.J., and Crowhurst, S., 1997. Sediment fluxes based on an orbitally tuned time scale 5 Ma to 14 Ma, Site 926. *In* Shackleton, N.J., Curry, W.B., Richter, C., and Bralower, T.J. (Eds.), *Proc. ODP, Sci. Results,* 154: College Station, TX (Ocean Drilling Program), 69–82.

Shackleton, N.J., Crowhurst, S., Hagelberg, T., Pisias, N.G., and Schneider, D.A., 1995b. A new late Neogene time scale: application to Leg 138 sites. *In* Pisias, N.G., Mayer, L.A., Janecek, T.R., Palmer-Julson, A., and van Andel, T.H. (Eds.), *Proc. ODP, Sci. Results,* 138: College Station, TX (Ocean Drilling Program), 73–101.

Shackleton, N.J., and Kennett, J.P., 1975. Late Cenozoic oxygen and carbon isotopic changes at DSDP Site 284: implications for glacial history of the Northern Hemisphere and Antarctica. *In* Kennett, J.P., Houtz, R.E., et al., *Init. Repts. DSDP,* 29: Washington (U.S. Govt. Printing Office), 801–807.

Sigurdsson, H., 1990a. Assessment of the atmospheric impact of volcanic eruptions. *Sp. Pap.—Geol. Soc. Am.,* 247:99–110.

————, 1990b. Evidence of volcanic loading of the atmosphere and climate response. *Palaeogeogr., Palaeoclimatol., Palaeoecol.,* 89:277–289.

Sigurdsson, H., Leckie, R.M., Acton, G.D., et al., 1997. *Proc. ODP, Init. Repts.,* 165: College Station, TX (Ocean Drilling Program).

Sigurdsson, H., Sparks, R.S.J., Carey, S.N., and Huang, T.C., 1980. Volcanogenic sedimentation in the Lesser Antilles arc. *J. Geol.,* 88:523–540.

Sinton, C.W., Duncan, R.A., Storey, M., Lewis, J., and Estrada, J.J., 1998. An oceanic flood basalt province at the core of the Caribbean plate. *Earth Planet. Sci. Lett.,* 155:222–235.

Smith, R.D., Cameron, K.L., McDowell, F.W., Niemeyer, S., and Sampson, D.E., 1996. Generation of voluminous silicic magmas and formation of mid-Cenozoic crust beneath north-central Mexico. *Contrib. Mineral. Petrol.,* 123:375–389.

Sugimura, A., Matsuda, T.C., Chinzei, T., and Nakamura, K., 1963. Quantitative distribution of late Cenozoic volcanic materials in Japan. *Bull. Volcanol.,* 26:125–140.

Verma, S.P., 1984. Sr and Nd isotopic evidence for petrogenesis of mid-Tertiary felsic volcanism in the mineral district of Zacatecas, Zac (Sierra Madre Occidental), Mexico. *Isotope Geol.,* 2:37–53.

von Huene, R., and Scholl, D.W., 1991. Observations at convergent margins concerning sediment subduction, subduction erosion, and the growth of the continental crust. *Rev. Geophys.,* 29:279–316.

Wiesemann, G., 1975. Remarks on the geologic structure of the Republic of El Salvador. *Mitt. Geol.-Palaeontol. Inst. Univ. Hamburg,* 44:557–574.

Worzel, J.L., Bryant, W., et al., 1973. *Init. Repts. DSDP,* 10: Washington (U.S. Govt. Printing Office).

Date of initial receipt: 10 February 1999
Date of acceptance: 27 August 1999
Ms 165SR-021